

UNIVERSITÄTSKLINIKUM HAMBURG-EPPENDORF

Institut für Experimentelle Pharmakologie und Toxikologie

Direktor: Prof. Dr. Thomas Eschenhagen

**Characterization of a human cellular model of desmin-related
cardiomyopathy**

Dissertation

zur Erlangung des Grades eines Doktors der Medizin an der Medizinischen
Fakultät der Universität Hamburg.

**vorgelegt von:
Jiancheng Cheng**

Hamburg 2022

Angenommen von der

Medizinischen Fakultät der Universität Hamburg am: 25.04.2023

Veröffentlicht mit Genehmigung der

Medizinischen Fakultät der Universität Hamburg.

Prüfungsausschuss, der/die Vorsitzende: Prof. Dr. Viacheslav Nikolaev

Prüfungsausschuss, zweite/r Gutachter/in: Prof. Dr. Lucie Carrier

Table of contents

1 Introduction	6
1.1 Desmin-related myopathy	6
1.1.1 The cytoskeleton structure	6
1.1.2 Involvement of α B-crystallin (<i>CRYAB</i>) in DRM	7
1.2 The protein quality control systems	8
1.2.1 The ubiquitin-proteasome system (UPS)	9
1.2.2 The autophagy-lysosomal pathway (ALP)	9
1.3 Aim of the project	10
2 Materials and Methods	11
2.1 Materials	11
2.1.1 Generation of mutant <i>CRYAB</i> human induced pluripotent stem cells (hiPSCs) ...	11
2.1.2 Cardiac differentiation of hiPSCs	11
2.2 Methods	12
2.2.1 Selection of hiPSC clones with <i>CRYAB</i> knock-in mutation	12
2.2.1.1 PCR amplification of genomic DNA	12
2.2.1.2 Agarose gel electrophoresis	13
2.2.1.3 PCR fragment purification	13
2.2.1.4 DNA sequencing of targeted hiPSC-clones	13
2.2.2 Determination of the <i>CRYAB</i> allele number in the <i>CRYAB</i> ^{hom} cell line	14
2.2.3 RNA analysis	14
2.2.3.1 RNA extraction	14
2.2.3.2 Determination of RNA concentrations	14
2.2.3.3 cDNA synthesis	15
2.2.3.4 Quantitative PCR	15
2.2.4 Protein analysis	17
2.2.4.1 Protein extraction	17

2.2.4.2 Determination of protein concentration	18
2.2.4.3 SDS-PAGE and Western blotting	19
2.2.5 Immunofluorescence	20
2.2.6 Statistical Analysis	21
3 Results	22
3.1 A CRYAB knock-in was identified in the selected hiPSC clones.	22
3.2 Two alleles in the CRYAB ^{hom} cell line were determined by qPCR assay.	24
3.3 Protein levels of CRYAB and DES were higher in ERC001 hiPSC-derived cardiomyocytes than that in hiPSCs	25
3.4 Protein levels of CRYAB and DES were significantly lower in CRYAB ^{hom} than in ERC001 hiPSC-CMs.	26
3.5 <i>CRYAB</i> and <i>DES</i> mRNA levels did not differ between CRYAB ^{hom} and ERC001 hiPSC-CMs at different time points.	28
3.6 Aggregate formation was detected in CRYAB ^{hom} hiPSC-CMs by immunofluorescence assay.	29
3.7 The autophagic flux was higher in 30-day-old CRYAB ^{hom} than ERC001 hiPSC- CMs	30
3.8 The autophagic flux did not differ between 60-day-old CRYAB ^{hom} and ERC001 hiPSC-CMs.	32
3.9 The UPS was impaired in 60-day-old CRYAB ^{hom} hiPSC-CMs	33
4 Discussion	36
4.1 The main aim and result of this project	36
4.2 Advantages of the CRISPR/Cas9 gene editing tools	36
4.3 Advantages of hiPSC-derived cardiomyocytes to study of heart diseases	37
4.4 Protein levels and aggregation of CRYAB and DES in DRM models	38
4.5 The UPS and ALP in DRM models	39
4.6 Limitations of the study	40

5 Summary	41
6 Zusammenfassung	43
7 References	45
8 List of tables	50
9 List of figures	51
10 Supplement	52
10.1 Abbreviations	52
10.2 Materials	54
10.2.1 Chemicals, reagents, drugs, etc.	54
10.2.2 Consumable materials	55
10.2.3 Laboratory equipment	56
10.2.4 Kits	56
10.2.5 Software	56
11 Acknowledgements	58
12 Curriculum Vitae	59
13 Eidesstattliche Versicherung	61

1 Introduction

1.1 Desmin-related myopathy

Desmin-related (cardio-)myopathy (DRM) is a protein-misfolding disease, characterized by conduction defects, skeletal muscle weakness and cardiomyopathy, which is caused by gene variants in desmin (*DES*), α B-crystallin (*CRYAB*) (Goldfarb et al. 2004, Clemen et al. 2015), myotilin (*MYOT*) (Selcen and Engel 2004), or filamin C (*FLNC*) (Vorgerd et al. 2005). Kedia et al. found that amyloid aggregates can be formed by the DES fragment 117–348 in physiological conditions (Kedia et al. 2019). Additionally, quite a lot of DRM samples are sporadic (van Spaendonck-Zwarts et al. 2011). Evidence showed that DRM can be restrictive, hypertrophic or dilated (Hnia et al. 2015). There is no specific therapy for desmin-related myopathy so far (Goldfarb et al. 2004). DRM shows a slow progression, over ten or twenty years, leading to the patients' severe disability, who need supporting therapies including pacemakers, wheelchairs, or respirators (Goudeau et al. 2001). The specific disease mechanism of DRM remains to be fully explored.

1.1.1 The cytoskeleton structure

The cytoskeleton functions as an integrated network comprising microtubules, intermediate filaments (IF) and microfilaments (Goldfarb et al. 2004). DES, the major muscle IF protein expressed in smooth skeletal and cardiac muscle, interplays with other proteins for the formation of a complex cytoskeletal network, which plays a crucial role in maintaining cellular integrity (Goldfarb and Dalakas 2009) (**Figure 1**).

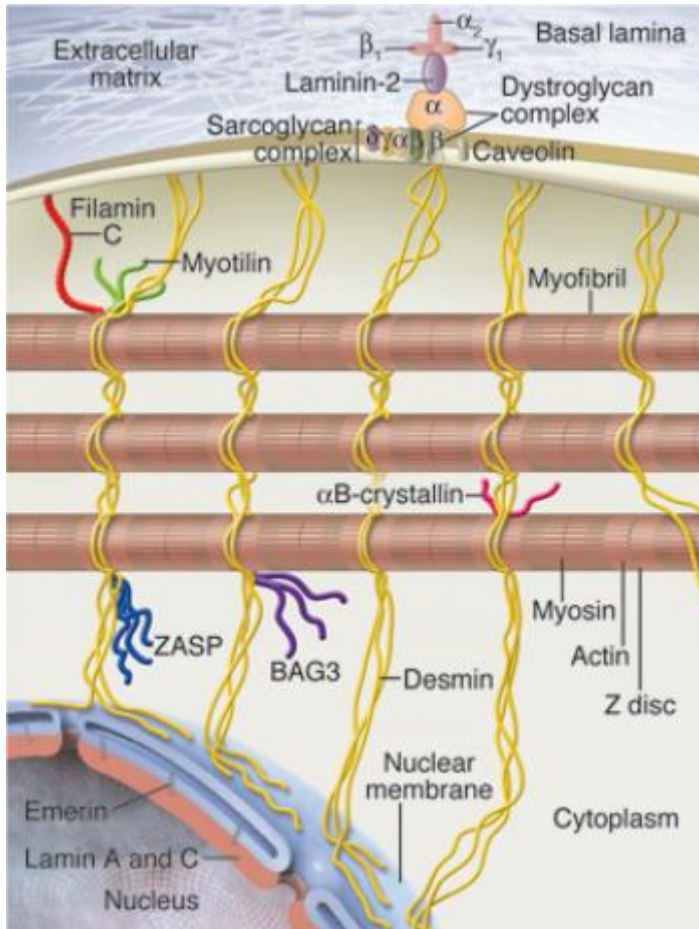


Figure 1: Molecular cytoarchitecture of myocyte, key proteins associated with cardiac and skeletal myopathies. Desmin, the major IF protein expressed in smooth skeletal and cardiac muscle interplays with other proteins for formation of a complex cytoskeletal network, which plays a crucial role in maintaining cellular integrity. α B-crystallin is a chaperone of *DES* that facilitates its proper folding. Figure adapted from Goldfarb et al. 2009.

1.1.2 Involvement of CRYAB in DRM

CRYAB is a small heat shock protein, which serves as a chaperone for proteins such as the IF protein DES, therefore helping to maintain cardiac muscle cell organization and function (Vicart et al. 1998). The R120G *CRYAB* mutation is associated with DRM, and has been shown to lead to the formation of enormous cytoplasmic CRYAB protein perinuclear aggregates in mice and iPSC-derived cardiomyocytes from transgenic mice (Wang et al. 2001, Limphong et al. 2013).

1.2 The protein quality control systems

The protein quality control (PQC) system can protect the cells from damage caused by abnormal

proteins through supporting protein folding as well as removing terminally misfolded proteins (Wang and Robbins 2006). The degradation of abnormal proteins in eukaryotic cells is mainly conducted by the two major protein degradation pathways: the ubiquitin-proteasome system (UPS) that functions to selectively degrade short-lived proteins (Voges et al. 1999, Smalle and Vierstra 2004) and the autophagy-lysosomal pathway (ALP) involved in degradation of bulk protein by engulfing and degrading organelles, damaged proteins and long-lived proteins (Mizushima and Klionsky 2007, Roberts and Deretic 2008) (**Figure 2**).

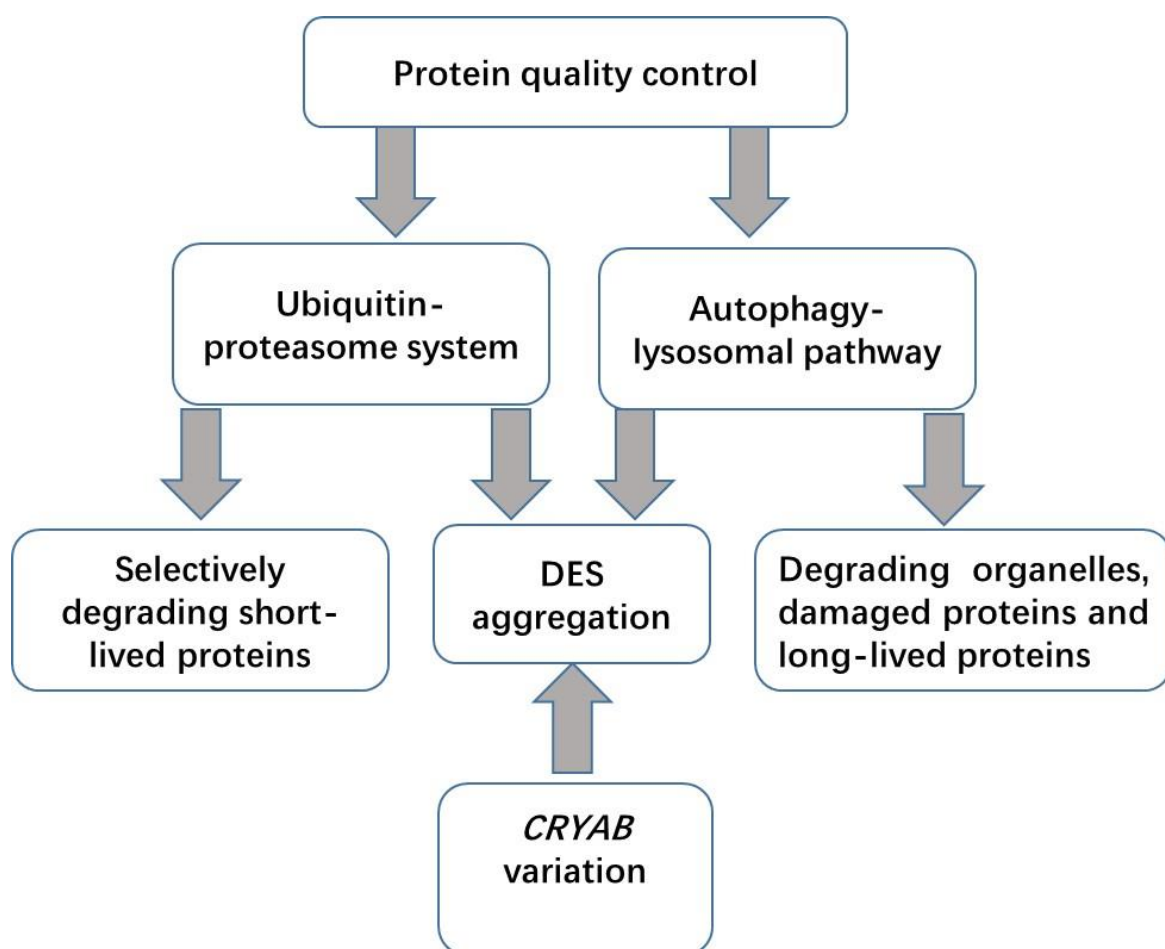


Figure 2. A scheme for protein quality control. Abbreviations: DES, desmin.

1.2.1 The ubiquitin-proteasome system

The UPS controls several essential biological processes including cell proliferation, cell death

as well as adaptation to stress, and its main role is to prevent the accumulation of damaged, mutant as well as misfolded proteins (Zolk et al. 2006). The UPS is highly selective in the degradation of most intracellular cytosolic, myofibrillar, and nuclear proteins. The initiation of protein degradation requires the covalent binding to the target protein of a chain comprising of a few ubiquitin copies via an enzymatic cascade that includes a ubiquitin-activating (E1) enzyme, a ubiquitin-conjugating (E2) enzyme and a ubiquitin-ligating (E3) enzyme (Hershko and Ciechanover 1998, Ravid and Hochstrasser 2008). The E3 ligases give the tissue-specificity to the system. Then, the poly-ubiquitinated target proteins are deubiquitinated, transferred to the proteasome and then degraded by specific enzymes in the proteasome core (Tanaka 2009, Schlossarek et al. 2014).

1.2.2 The autophagy-lysosomal pathway

Autophagy serves as a complex process by which proteins or cytoplasmic components are shuttled to the lysosome for degradation (Yim and Mizushima 2020). Autophagy primarily contains three forms: macroautophagy, chaperone-mediated autophagy as well as microautophagy (Mizushima et al. 2008). Macroautophagy is often known as ALP (Levine and Kroemer 2008). Microtubule-associated protein light chain 3 (LC3), a mammalian homologue of Apg8p critical to autophagy in yeast, contains two forms: LC3-I and LC3-II. LC3-I is in the cytoplasm, which can be lipidated to LC3-II after autophagic activation. LC3-II is integrated in the autophagosomal membrane and shows a punctate distribution by microscopy, which indicates the existence of autophagic vacuoles. As a consequence, LC3-II functions as an autophagosomal marker (Kabeya et al. 2000). Autophagy can be detected by assessing the levels of autophagy-associated proteins or via evaluating the autophagic activity/flux. The levels of LC3-II can provide a hint as to whether the autophagic pathway is abnormally modulated. Elevated protein levels of LC3-II suggest either autophagosome formation is increased or autophagosome clearance is impaired, indicating that when autophagic flux was high, level of LC3-II was low (Zech et al. 2020). Additionally, Klionsky et al. suggested that a high level of p62 was a marker of impairment of autophagic flux (Klionsky et al. 2021).

1.3 Aim of the project

The main aim of this project was to characterize a novel human induced pluripotent stem cell (hiPSC)-derived DRM model with the *CRYAB* R120G mutation, which was created in the institute with the CRISPR/Cas9 gene editing tools.

2 Materials and Methods

2.1 Materials

2.1.1 Generation of mutant *CRYAB* human induced pluripotent stem cells (hiPSCs)

This part was performed by Niels Pietsch using the clustered regularly interspaced short palindromic repeat/CRISPR-associated Cas9 (CRISPR/Cas9) genetic tools from a control hiPSC line (ERC001). The goal was to introduce in the ERC001 hiPSC line a heterozygous missense mutation in the *CRYAB* locus to create the *CRYAB*^{hom} mutant hiPSC line (c.358A>G; p.R120G; *CRYAB*^{hom}). In brief, the ribonucleic protein (RNP) containing Cas9 and a single guide RNA (sgRNA: 5'-UCAUCUCCAGGGAGUCCAC-3') were assembled. Then, nucleofection was performed with RNP complex and single-stranded DNA oligonucleotides (ssODN) containing the *CRYAB*-mutated sequence in ERC001 hiPSCs, and the cells were set to recover. Following this, the cells were seeded. Then, puromycin selection was conducted before clones of single cells were expanded (Paquet et al. 2016, Roberts et al. 2017). Validation of the *CRYAB*^{hom} hiPSC line is described in the 2.2.1 section.

2.1.2 Cardiac differentiation of hiPSCs

The *CRYAB*^{hom} and ERC001 hiPSCs were differentiated into cardiomyocytes (CMs) (=hiPSC-CMs) by Niels Pietsch and Antonietta Fazio using a monolayer protocol as described previously (Breckwoldt et al. 2017)(Mosqueira et al. 2018). In brief, the hiPSCs were thawed about a week before the onset of differentiation. Expansion was performed for 2 to 3 passages according to the CM number required finally. Seeding densities of the cells varied from 300,000 to 500,000 per well and cells were cultured until they reached confluence of 60-70 %. After that, cardiomyocyte-differentiation was induced. The differentiation process following induction took about 14 days. To guarantee reliable programming of hiPSCs into differentiated CMs, a few media that contained different growth factors were added at very specific time points. After 30 days and 60 days of differentiation, respectively, cell pellets for protein extraction were obtained. After 7 days, 30 days, 40 days and 60 days of differentiation,

respectively, cell pellets for RNA extraction were collected.

2.2 Methods

2.2.1 Selection of hiPSC clones with *CRYAB* knock-in mutation

2.2.1.1 PCR amplification of genomic DNA

First, genomic DNA (gDNA) was isolated from hiPSC pellets of the obtained clones using DNeasy Blood Tissue Kit (250) (QIAGEN) according to the manufacturer's instructions. Second, a PCR amplification of genomic DNA was conducted using a PCR kit (Thermo Fisher Scientific). Substances for the PCR are listed in **Table 1**. PCR program is shown in **Table 2**. The PCR primers are shown in **Table 3**.

Table 1: PCR mixture

Component	Volume for 20 μ L approach (μ l)
10 x buffer	2
dNTP (10 mM)	0.4
Taq (250 units)	0.2
MgCl ₂ (25 mM)	1.2
H ₂ O	14.4
gDNA	1
Primer FW (200 nM)	0.4
Primer Rev (200 nM)	0.4

Abbreviations: FW, forward; Rev, reverse.

Table 2: PCR program for genomic DNA amplification

PCR step	Temperature in C°	Time	Cycles
Initialization	95	5 min	1
Denaturation	95	30 sec	11
Annealing	61	30 sec	11
Elongation	72	1 min	11
Denaturation	95	30 sec	25
Annealing	56	30 sec	25
Elongation	72	1 min	25
Final hold	72	7 min	1

Table 3: PCR primers

Primer	Primer sequence (5'-3')
<i>CRYAB</i> FW (200 nM)	CTTGAGAGTCAGCAGGCA
<i>CRYAB</i> Rev (200 nM)	GCTTCAGCACTAGTCACAAGAC

Abbreviations: *CRYAB*, α B-crystallin; FW, forward; Rev, reverse.

2.2.1.2 Agarose gel electrophoresis

Agarose gel electrophoresis assay was carried out with PCR products. Samples were mixed with a 6x loading dye and separated on 1% agarose gel (in Tris-acetate-EDTA (TAE) buffer with the Midori Green Advance DNA Stain (**Table 4**). Agarose gels (1%) were run in 1x TAE running buffer at 120 V for 40 min to determine the fragment size. GeneRuler 1 kb DNA Ladder served as the molecular weight marker.

Table 4: Agarose gel mixture

Agarose	1.5 g
Midori Green Advance DNA Stain	7 μ l
TAE	150 ml

Abbreviations: TAE, tris acetate ethylenediaminetetraacetic acid.

2.2.1.3 PCR fragment purification

PCR bands were extracted from the agarose gel and purified with the QIAquick® PCR Purification Kit according to the manufacturer's instructions. The DNA was eluted in 20 μ l H₂O and subsequently stored at -20 °C.

2.2.1.4 DNA sequencing of targeted hiPSC clones

Two μ l of reverse primer for *CRYAB* were mixed to 75 ng purified PCR fragments and H₂O to a final volume of 17 μ l that was used for gDNA sequencing. Sequencing was performed by the Eurofins company.

2.2.2 Determination of the *CRYAB* allele number in the CRYABhom cell line

Quantitative PCR (qPCR) assay on genomic DNA (gDNA) was performed to detect the number of *CRYAB* alleles in the CRYABhom hiPSC line. The primers located in the *CRYAB* gene were used for the qPCR. The gDNA of CRYABhom and ERC001 hiPSCs was diluted into 1:2, 1:5, 1:10, 1:15 and 1:20, respectively. For each diluted group, the CT value of *CRYAB* gene was normalized to the CT value of nuclear respiratory factor 1 (*NRFI*) gene and then the CT value of CRYABhom hiPSCs was related to the CT value of ERC001 hiPSCs. Y axis represented the number of alleles.

2.2.3 RNA analysis

2.2.3.1 RNA extraction

RNA was extracted from CRYABhom and ERC001 hiPSC-CMs by using the TRIzol reagent (Promega) in accordance to the manufacturer's instructions. Firstly, 0.5 ml TRIzol was added to each tube for homogenization at room temperature. Following this, 0.1 ml of chloroform was added to each tube and incubated for 3 min at room temperature. Then, the samples were centrifuged at 13200 rpm for 30 min at 4 °C. After removing the aqueous phase through angling the tube at 45°, the aqueous phase was placed into a new tube. For RNA extraction, 0.25 ml isopropanol was added into the aqueous phase for each tube for homogenization and then for incubation for 10 min at room temperature. After this, the tubes were centrifuged at 13200 rpm for 20 mins at 4 °C. Following that, the supernatant was removed from the tube and only the RNA pellet was left. Next, 0.5 ml of 75% ethanol was added into each tube for homogenization and then centrifuged at 13200 rpm for 20 min at 4 °C. The supernatant was discarded and the RNA pellet was air-dried for 5-10 min. At last, the RNA pellet was resuspended in 20 µl of RNase-free water for each tube. The total extracted RNA was stored at -80 °C for further use.

2.2.3.2 Determination of RNA concentrations

The quality and concentration of RNA were determined by the NanoDrop™ ND-1000 spectrophotometer. The absorbance was measured at a wavelength of 260 nm. The system

suggests that every unit of absorbance is corresponding to 40 µg/mL of RNA. The ratio of absorbance at 260 nm and 280 nm was applied to evaluate the purity of RNA and a ratio of 1.8-2.0 served as accepted purity for RNA. If the ratio was lower than 1.8, it may suggest the contamination of protein, phenol or other contaminants.

2.2.3.3 cDNA synthesis

Two hundred ng of RNA was used for cDNA Synthesis by the iScript™ cDNA Synthesis Kit (Bio Rad) in accordance to the manufacturer's instructions. The program of cDNA synthesis was carried out according to the protocol in **Table 5**. Components for cDNA synthesis are listed in **Table 6**.

Table 5: Program for cDNA synthesis

Step	Temperature in C°	Time
Step 1	25	5 min
Step 2	46	20 min
Step 3	95	1 min
Final hold	4	-

Table 6: Components for cDNA synthesis

Component	Volume (µL)
RNA	Volume of 200 ng RNA
H ₂ O	16 - Volume of 200 ng RNA
5x iScript Mix	4
Total volume	20

2.2.3.4 Quantitative PCR (qPCR)

Dilutions (1:10) of cDNA were prepared as starting material. After that, PCR was performed with a qPCR kit (ThermoScientific) based on TaqManR ABI PrismR7900HT sequence detection system. mRNA was normalized to beta glucuronidase (*GUSB*) and the relative gene expression was assessed by the $2^{-\Delta\Delta C_t}$ method. Each experiment was performed in triplicate. The PCR program is depicted in **Table 7** and the primers are shown in **Table 8**. The components

for the qPCR are shown in **Table 9**.

Table 7: Program for qPCR

PCR step	Temperature in C°	Time	Cycles
Stage 1	50	2 min	1
Stage 2	95	10 min	1
Stage 3	95	15 sec	40
Stage 3	60	1 min	40
Stage 4	95	15 sec	1
Stage 4	60	15 sec	1
Stage 4	95	15 sec	1

Table 8: Primers for qPCR

Primer	Primer sequence (5'-3')
<i>CRYAB</i> FW	CGCCCTTCTTTCTTTCCA
<i>CRYAB</i> Rev	GAACCTGTCCTTCTCCAGGC
<i>DES</i> FW	GCAGCTACTCTAGCTCGCAT
<i>DES</i> Rev	TGTTCTGAAGCTGAGCCTG
<i>GUSB</i> FW	ACGATTGCAGGGTTTCACCA
<i>GUSB</i> Rev	CACTCTCGTCGGTGACTGTT

Abbreviations used: *CRYAB*, α B-crystallin; *DES*, desmin; FW, forward; *GUSB*, beta glucuronidase; Rev, reverse.

Table 9: Components of qPCR

Component	Volume (μ L)
SYBR green (Mix)	5
H ₂ O	2.2
cDNA (1:10)	1
Primer FW (900 nM)	0.9
Primer Rev (900 nM)	0.9
Total volume	10

Abbreviations: FW, forward; Rev, reverse.

2.2.4 Protein analysis

2.2.4.1 Protein extraction

A flow diagram for Western blot of the cells is shown in **Figure 3**. A solution of 100 μ l (1 protease inhibitor tablet in 10 ml Millipore water) was added into each Eppendorf tube containing hiPSC-CM pellet. Next, the samples were homogenized by pipetting up and down several times and then centrifuged at 13200 rpm for 30 min at 4 °C using a centrifuge (Eppendorf 5810 R). After that, the supernatant was collected as cytosolic fraction in a new tube. Then, 100 μ l solution (1 M dithiothreitol (DTT) was diluted 1:1000 into SDS buffer (**Table 10**)) was added to each cell pellet and the samples were homogenized via pipetting up and down a few times. Following this, the samples were centrifuged at 13200 rpm, 15 min at 18-20 °C and the supernatant was used as SDS fraction in a new tube. Then, 25 μ l of 8 M urea solution (Tris 50 mM, pH 7.4) was added to pellets and the samples were resuspended through pipetting up and down several times. Afterwards, the protein extract was sonicated (50-60 W) 2x 7 sec, which was applied as urea fraction. If the extract was still cloudy, the above step was repeated once. The protein extract was sonicated again before gel electrophoresis.

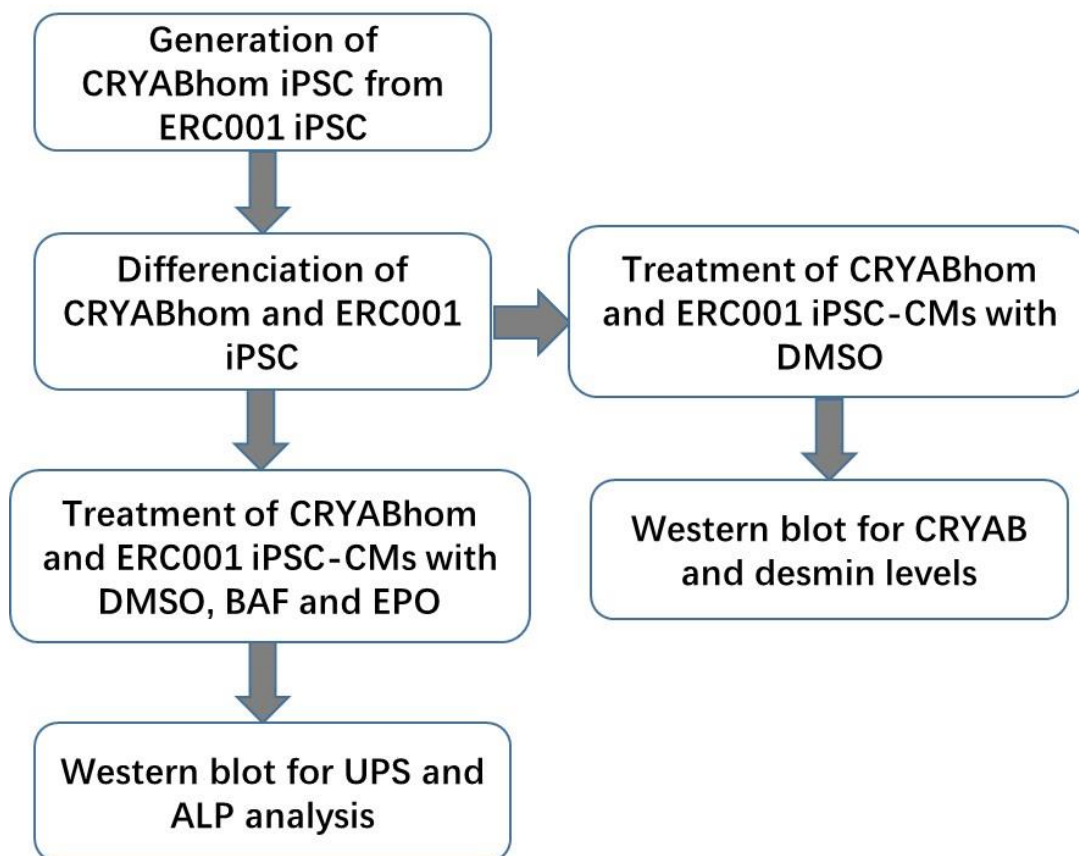


Figure 3. A flow diagram for Western blot of the cells.

Abbreviations: ALP, autophagy-lysosomal pathway; BAF, bafilomycin A₁ (50 nM); DMSO, dimethylsulfoxide; EPO, epoxomicin (250 nM).

Table 10: SDS buffer

SDS buffer	2 mL Tris (1.5 M, pH 8.8)
	1 mL EDTA (0.5 M)
	6 mL NaF (500 mM)
	15 mL SDS (20%)
	10 mL Glycerol
	Add H ₂ O to 100 mL

Abbreviations: EDTA, ethylenediaminetetraacetic acid; NaF, sodium fluoride; SDS, sodium dodecyl sulfate.

2.2.4.2 Determination of protein concentration

The protein concentration of the obtained samples (66 samples) was measured by Qubit™ Protein Assay Kit, 500 assays (Invitrogen) and calculated in the Qubit Fluorometer 3.0 (Invitrogen) in accordance to the protocol of the manufacturer.

2.2.4.3 SDS-PAGE and Western blotting

The samples were mixed with 6x Laemmli buffer (10% glycerol, 0.01% bromophenol blue, 10 mM Tris base, pH 6.8, 100 mM DTT, 2% SDS) and denatured at 55 °C for 10 min or at 95 °C for 5 min. After that, the samples (7-16 µg per lane) were subjected to 8%, 10% or 12% SDS polyacrylamide gel electrophoresis (SDS-PAGE), according to the experiment. The BenchMark Protein Ladder (Thermo Fisher Scientific) was employed as a molecular weight marker for the SDS-PAGE. Following this, the proteins were transferred onto polyvinyl-difluoride (PVDF; GE Healthcare) or nitrocellulose (NC; Amersham™) membranes through wet-electroblotting at 400 mA for 50 min or 350 mA for 80 min in a mini Trans-blot chamber (Bio-Rad) system. To detect the transfer quality, the NC membranes were stained using Ponceau S solution (Sigma) for 10 min. After visualizing the signal of all the protein, the membranes were washed 3x for 5 min with 1x TBS-Tween 0.1% (TBS-T) and blocked with 5% milk powder in TBS-T solution for 1 h. Afterwards, the membranes were washed 3x 5 min with 1x TBS-T 1% and then stained with the primary antibody (**Table 11**) at 4 °C overnight. The membranes were then washed 3x with 1x TBS-T 0.1% and then incubated for 1.5 h with the secondary antibody (**Table 11**) at room temperature. Finally, the electrochemiluminescence (ECL) was applied to visualize the proteins and protein bands of the blots were quantified by the band analysis tool of ImageLab (Bio-Rad Laboratories).

Table 11: Primary and secondary antibodies for Western blot

Protein name	Primary antibody	Company (catalog number)	Dilution	Secondary antibody	Company	Dilution
CRYAB	CRYAB	Santa Cruz (ADI-SPA-222)	1/1000	Anti-mouse IgG	Sigma	1/10000
DES	DES	Millipore (04-585)/Sigma-Aldrich (SAB5600054)	1/1000	Anti-rabbit IgG	Sigma	1/10000
LC3-II	LC3-II	Cell Signaling (2775)	1/1000	Anti-rabbit IgG	Sigma	1/10000
p62	p62	Sigma (P0067)	1/2000	Anti-rabbit IgG	Sigma	1/10000
Ubiquitin/Poly ubiquitin	Ubiquitin	Biomol (Enzo life sciences) (BML-PW 8810)	1/10000	Anti-mouse IgG	Sigma	1/10000
GFP/GFPu	GFP	Santa Cruz (sc-8334)	1/5000	Anti-rabbit IgG	Sigma	1/10000
ACTN2	ACTN2	Sigma (A7811)	1/10000	Anti-mouse IgG	Sigma	1/10000
GAPDH	GAPDH	HyTest (5G4)	1/5000	Anti-mouse IgG	Sigma	1/10000

2.2.5 Immunofluorescence

Cells were washed 3 times by using 1x PBS and then fixed with Roti-Histofix (4% phosphate-buffered paraformaldehyde (PFA)) at 4 °C for 20 min. After this, cells were washed 2 times with 1x PBS. Following that, cells were permeabilized by using 0.5% TritonX100 in PBS for 20 min and then washed 3 times by using 1x PBS. Next, the cells were blocked with 5% bovine serum albumin (BSA) in PBS-T for 30 min and then incubated with primary antibodies mouse anti-CRYAB (1:100 dilution), mouse anti- α -actinin 2 (ACTN2) monoclonal antibodies (1:800 dilution) and rabbit anti-DES (1:100 dilution) monoclonal antibodies overnight at 4 °C. Cells were then washed 2 times with 1x PBS-T and then incubated with a 1:100 dilution of rabbit anti-mouse IgG and mouse anti-rabbit IgG for 2 h at room temperature in the dark. Finally, the cells were washed 3 times by using 1x PBS and then stained with DAPI (Hoechst 33342, 1:2000) for 20 min, washed 3 times using 1x PBS. Finally, the samples were observed under an

immunofluorescence microscope. The immunofluorescence assay was performed by Antonietta Fazio.

2.2.6 Statistical Analysis

Data are expressed as mean \pm standard error of mean (SEM) and difference between groups was analyzed with GraphPad Prism software 8.0, using unpaired Student's t-test or two-way ANOVA when appropriate. $P < 0.05$ was considered to be statistically significant.

3 Results

3.1 A *CRYAB* knock-in was identified in the selected hiPSC clones

To create a human cellular model of DRM, the c.358A>G (R120G) mutation was introduced in ERC001 hiPSC line with CRISPR/Cas9 genetic tools via a template containing the c.358G mutation and 2 specific sgRNAs targeted to the *CRYAB* locus. This was done by Niels Pietsch in the institute. To evaluate the consequence of CRISPR/Cas9, recombinant hiPSC clones were evaluated by genomic PCR in *CRYAB* exon 4 and sequencing. **Figure 4** shows the outcomes of agarose gel electrophoresis of PCR products of the selected clones. PCR products of gDNA with *CRYAB*-specific primers were observed at the length of 947 bp and no band in the negative control.

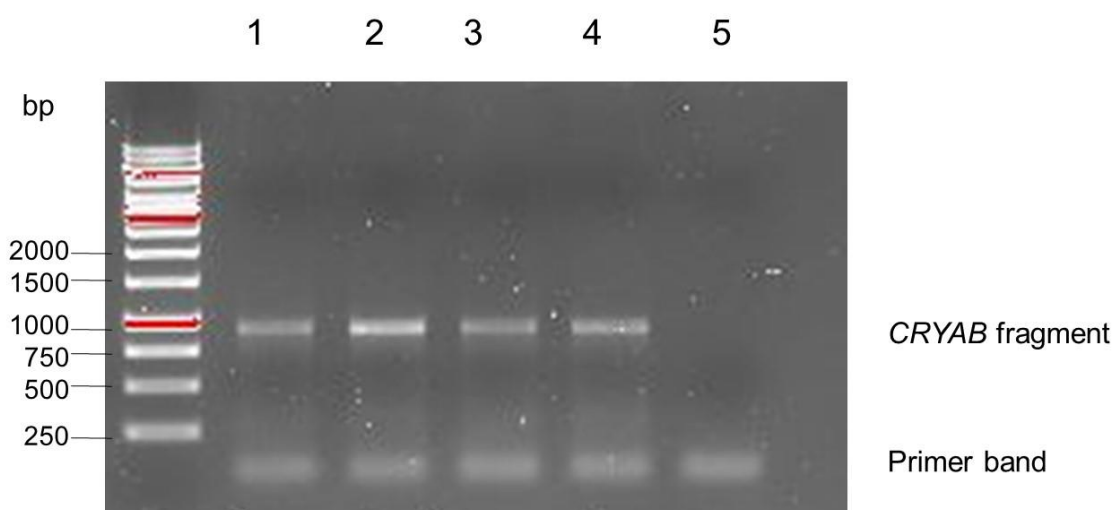


Figure 4. Agarose gel electrophoresis of genomic PCR products of the selected hiPSC clones. The genomic DNA from hiPSC pellets of selected clones was used for PCR using *CRYAB* primers. Then, 10 μ l PCR product was mixed with 6x loading dye for each sample and then separated on 1% agarose gel with the DNA intercalator MIDORIGreen in 1x TAE running buffer at 120 V for 40 min. GeneRuler 1 kb DNA Ladder was the molecular weight marker and the size of *CRYAB* fragment was 947 bp. Ten μ l PCR product was used to lanes 1, 2, 3, and 4, respectively and 10 μ l H₂O was applied to lane 5 as blank control.

Sequencing of the PCR products was then conducted (**Figure 5**). First, the sequence shows a variation on position 358 bp of the coding sequence of the *CRYAB* transcript (NCBI: NM_001289807.1), where an adenine was replaced by a guanine (c.358A>G) on both alleles. The mutation resulted in an amino acid change on position 120 (arginine to glycine; R120G). Second, the sequence also shows another variation on position 360 bp of the *CRYAB* transcript, where a guanine was replaced by an adenine on both alleles. This variation was introduced in the template for homology directed repair to confirm the insertion and the zygosity state. This is a silent gene variant, which does not affect the amino acid. Therefore, this data suggests that CRISPR/Cas9 introduced a homozygous c.358A>G (R120G) mutation and could be used as a human cellular model of DRM. This cell line was thus named CRYABhom.

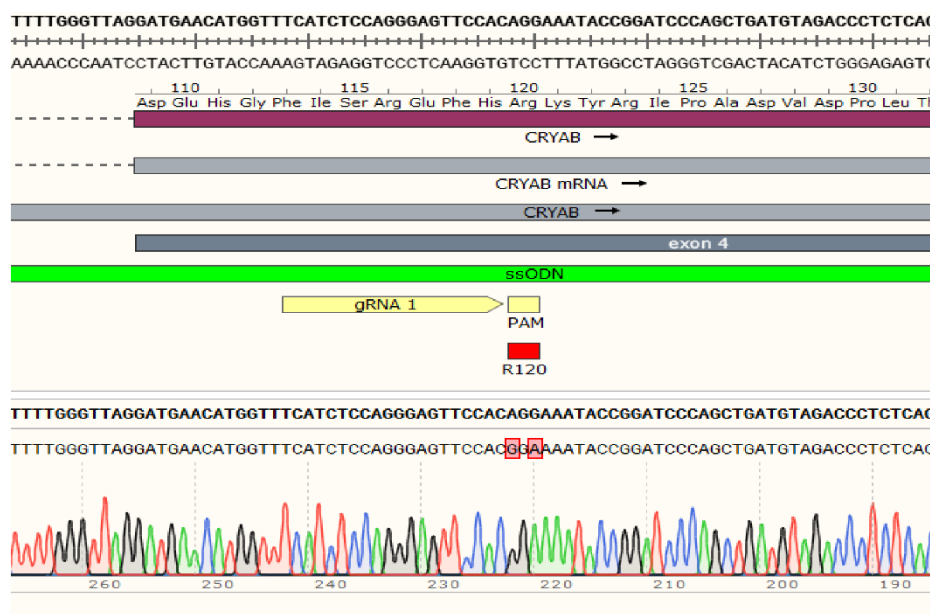


Figure 5. Sequencing of the recombinant *CRYAB*-targeted hiPSC clone. Genomic DNA extracted from hiPSC clone cell pellets was used for PCR using the primers for *CRYAB* and 10 μ l PCR product was used for PCR fragment purification. Then, 2 μ l reverse primer for *CRYAB* was mixed to 75 ng of purified PCR fragments in H₂O to a final volume of 17 μ l for DNA sequencing. The amplified sequencing showed a point mutation on position 358 bp which represented the coding sequence of the *CRYAB* transcript variant (NCBI: NM_001289807.1), where an adenine was replaced by a guanine on both alleles. The mutation resulted in an amino acid change (arginine to glycine). The amplified

sequencing also showed a point mutation on position 360 bp that stood for the coding sequence of the *CRYAB* transcript variant (NM_001289807.1), where a guanine was replaced by an adenine on both alleles. While the change from guanine into adenine was a silent mutation.

3.2 Two alleles in the CRYABhom cell line were determined by qPCR assay

To evaluate whether the introduced mutation (c.358A>G; R120G) is homozygous and not associated with a deletion of the other allele, qPCR was performed to determine the number of alleles in the CRYABhom hiPSC line. Various dilutions of gDNA were used and *CRYAB* was compared to nuclear respiratory factor 1 (*NRF1*; **Figure 6A**). The CT values of *CRYAB* decreased in a concentration-dependent manner and were similar to those of *NRF1* in CRYABhom hiPSC line. A similar result was observed in ERC001 hiPSC line (**Figure 6B**). As for the CRYABhom hiPSC line, the corresponding allele number of the groups whose concentrations were diluted into 1:20, 1:15, 1:10, 1:5 and 1:2, were 2.9, 2.1, 2.0, 2.2, and 2.0, respectively (**Figure 6B**). The allele number of group whose concentration was diluted into 1:20, was a bit higher than that in the other groups, possibly due to the effect of a low concentration of the samples. Collectively, two alleles in the CRYABhom hiPSC cell line were identified by qPCR assay using gDNA of CRYABhom and ERC001 hiPSC lines.

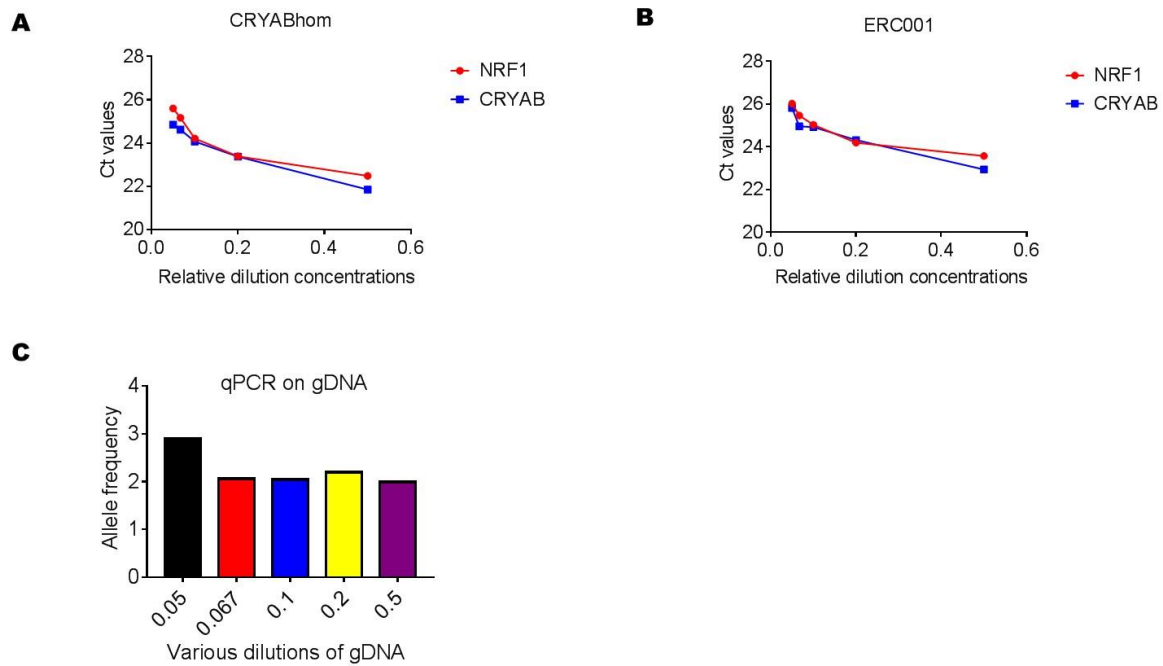


Figure 6. qPCR assay for determination of the allele number in the CRYABhom hiPSC line. The primers were located in *CRYAB* and *NRF1* genes. The gDNA of CRYABhom and ERC001 hiPSCs was diluted into 1:2, 1:5, 1:10, 1:15 and 1:20. **A)** CT values of *CRYAB* are depicted on the Y axis; CRYABhom hiPSC gDNA samples with different relative concentrations are depicted on the X axis. **B)** CT values of *CRYAB* are shown on the Y axis; ERC001 hiPSC gDNA samples with different relative concentration are shown on the X axis. **C** Y axis represented the number of alleles; X axis stood for samples with different relative concentrations. gDNA: Genomic DNA.

Then, pluripotency assay for the CRYABhom hiPSC line was performed by Niels and confirmed.

3.3 Protein levels of CRYAB and DES were higher in ERC001 hiPSC-derived cardiomyocytes than in hiPSCs

ERC001 hiPSC line was then differentiated into cardiomyocytes (=hiPSC-CMs) and cultivated for 30 days. Protein extractions were separated in cytosolic, SDS and urea fractions. First, Western blot was performed to assess the protein levels of CRYAB and DES in both hiPSCs and hiPSC-CMs from the ERC001 line. **Figure 7** shows the representative Western blot

(CRYAB, DES; 12% SDS gel) of the SDS fraction of hiPSC-CMs and hiPSCs with or without dimethylsulfoxide (DMSO). Ponceau was used as loading control, indicating that the protein levels of CRYAB (apparent molecular weight of 20 kDa) and DES (apparent molecular weight of 53 kDa) were significantly higher in ERC001 hiPSC-CMs than in hiPSCs.

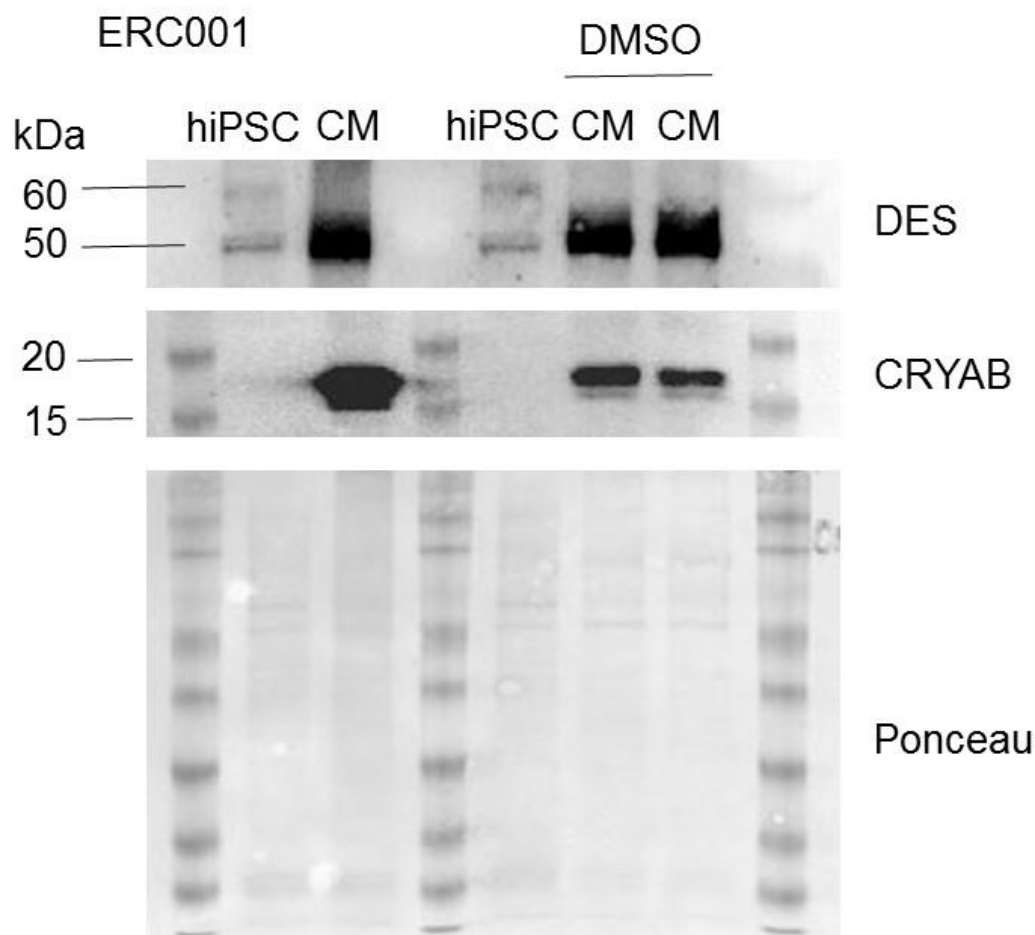


Figure 7. Western blot assay for CRYAB and DES protein levels of ERC001 hiPSCs and hiPSC-CMs. Western blot (CRYAB, DES; 12% SDS gel) of the SDS fraction of ERC001 hiPSCs and hiPSC-CMs with or without DMSO. Ponceau was used as loading control. Abbreviations: DMSO, dimethylsulfoxide; CM, human induced pluripotent stem cell-derived cardiomyocytes; hiPSC, human induced pluripotent stem cell. DES, desmin.

3.4 Protein levels of CRYAB and DES were significantly lower in CRYAB^{hom} than in ERC001 hiPSC-CMs

We then compared the levels of CRYAB and DES between CRYABhom and ERC001 hiPSC-CMs at 30 days of culture. **Figure 8A** exhibits a representative Western blot (CRYAB, DES; 12% SDS gel) of the cytosolic, SDS and urea fraction of CRYABhom and ERC001 hiPSC-CMs with or without DMSO at 30 days. α -Actinin-2 (ACTN2), glyceraldehyde-3-phosphate dehydrogenase (GAPDH) and Ponceau were used as loading controls. Most of ACTN2, CRYAB and DES proteins were extracted with the SDS fraction, though some were found in the cytosolic and urea fractions. **Figure 8B, 8C** shows that the protein levels of CRYAB and DES were lower in CRYABhom than in ERC001 hiPSC-CMs.

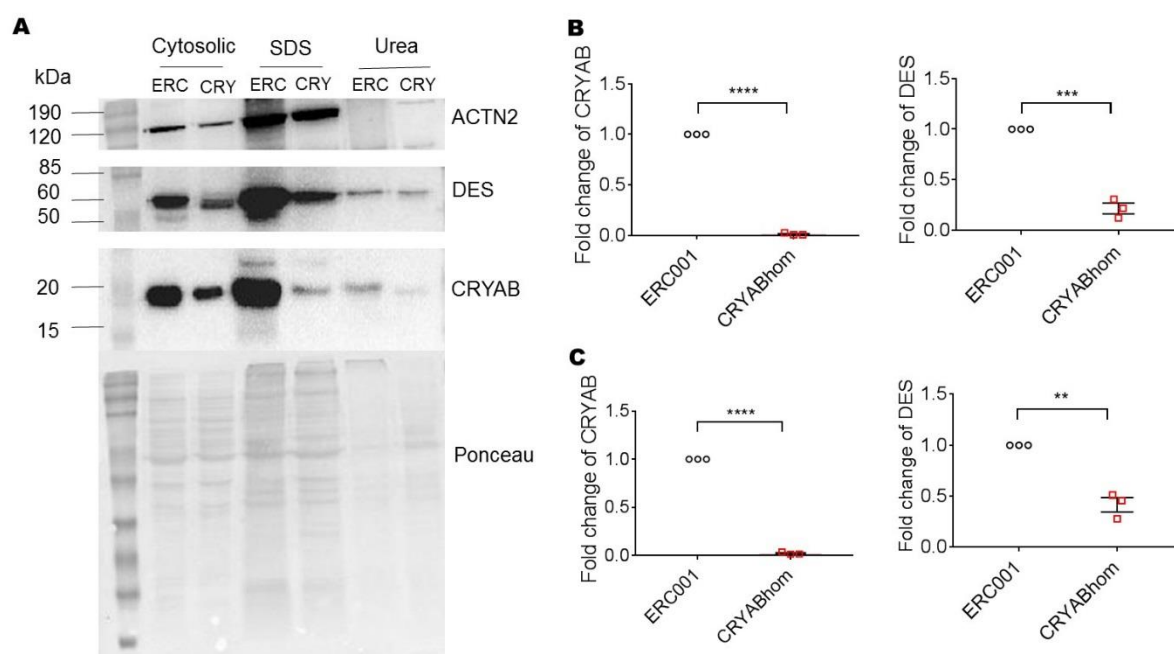


Figure 8. Quantification of the protein levels of CRYAB and DES in CRYABhom and ERC001 hiPSC-CMs at 30 days. A Representative Western blot (CRYAB, DES; 12% SDS gel) of the cytosolic, SDS and urea fraction of CRYABhom and ERC001 hiPSC-CMs with or without DMSO at 30 days. **B & C** Quantification of Western blots. Data are expressed as mean \pm SEM, with **P < 0.01, ***P < 0.001 and ****P < 0.0001, unpaired Student's t-test (n=3 biological replicates). ACTN2, GAPDH (**B**) and Ponceau (**C**) were used as loading controls for both CRYAB and DES. Abbreviations: CRY, CRYABhom; DMSO, dimethylsulfoxide; ERC, ERC001; GAPDH, glyceraldehyde-3-phosphate dehydrogenase; ACTN2, α -actinin 2; DES, desmin.

3.5 *CRYAB* and *DES* mRNA levels did not differ between *CRYAB*hom and ERC001 hiPSC-CMs at different time points

To evaluate whether the lower levels of both *CRYAB* and *DES* proteins were due to a lower transcription in *CRYAB*hom hiPSC-CMs, RT-qPCR assay was used to evaluate the mRNA levels of *CRYAB* and *DES* in *CRYAB*hom and ERC001 hiPSC-CMs at different time points of culture. Both *CRYAB* and *DES* mRNA levels increased with culture time in ERC001, but the difference was not significant, likely due to the low number of biological replicates (**Figure 9A, 9B**). Furthermore, mRNA levels of *CRYAB* and *DES* did not differ between *CRYAB*hom and ERC001 hiPSC-CMs at different time points (**Figure 9C & 9D**). This suggests that the lower level of *CRYAB* and *DES* proteins (**Figure 8**) results from a post-transcriptional regulation in *CRYAB*hom hiPSC-CMs.

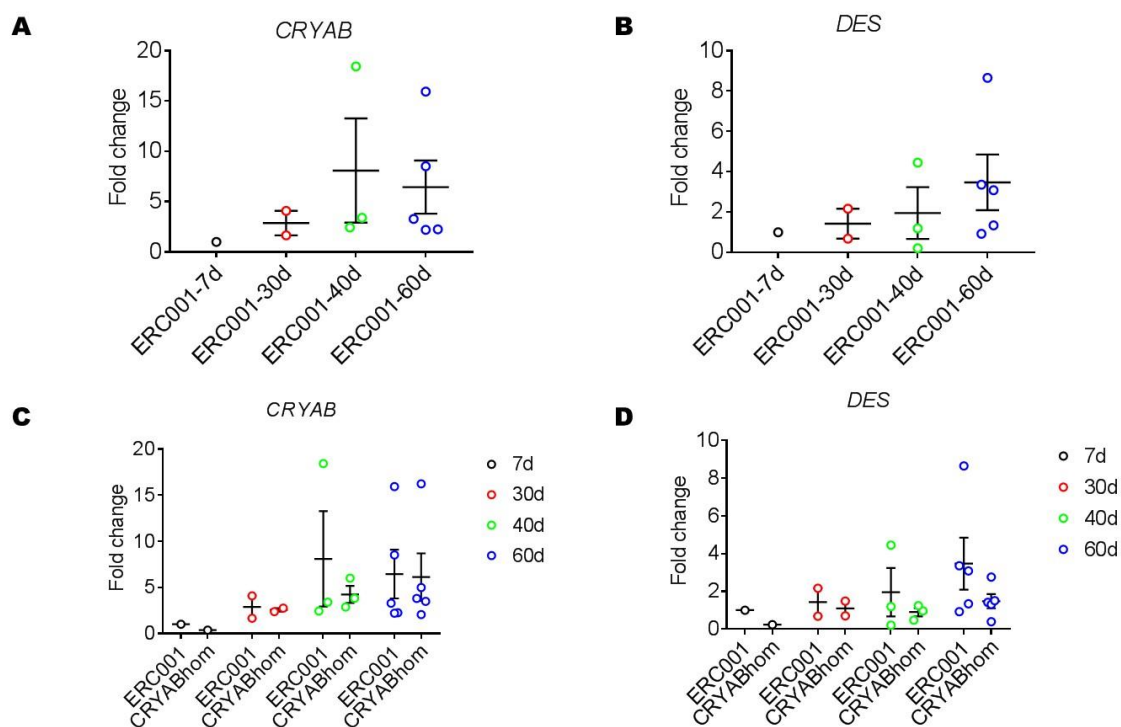


Figure 9. Determination of mRNA levels of *CRYAB* and *DES* in *CRYAB*hom and ERC001 hiPSC-CMs at different time points. RT-qPCR for *CRYAB* (**A**) and *DES* (**B**) was performed from extracted RNA of ERC001 hiPSC-CMs at 7 days, 30 days, 40 days and 60 days, respectively. *GUSB* was used as

housekeeping gene. **(C & D)** Comparison of RT-qPCR between both cell lines at 7 days, 30 days, 40 days and 60 days. GUSB was used as housekeeping gene. Abbreviations: CRYAB, α B-crystallin; GUSB, beta glucuronidase; DES, desmin; hiPSC-CMs: human induced pluripotent stem cell-derived cardiomyocytes.

3.6 Aggregate formation was detected in CRYAB^{hom} hiPSC-CMs by immunofluorescence assay

Immunofluorescence assay was used to assess aggregate formation in CRYAB^{hom} hiPSC-CMs. **Figure 10A** shows well organized striated myofibril structures for ACTN2 and low signal intensity for CRYAB in ERC001 hiPSC-CMs. On the other hand, ACTN2 staining was disorganized and exhibited spotted sarcomere structures and CRYAB intensity was stronger and aggregated in CRYAB^{hom} hiPSC-CMs. **Figure 10B** shows a well-organized sarcomere structure stained for both ACTN2 and DES in ERC001 hiPSC-CMs. Interestingly, only one of the two cardiomyocytes was positively stained for *DES*, suggesting that the differentiation is not fully synchronized. Furthermore, ACTN2 striations were visible, but DES formed aggregates in CRYAB^{hom} hiPSC-CMs.

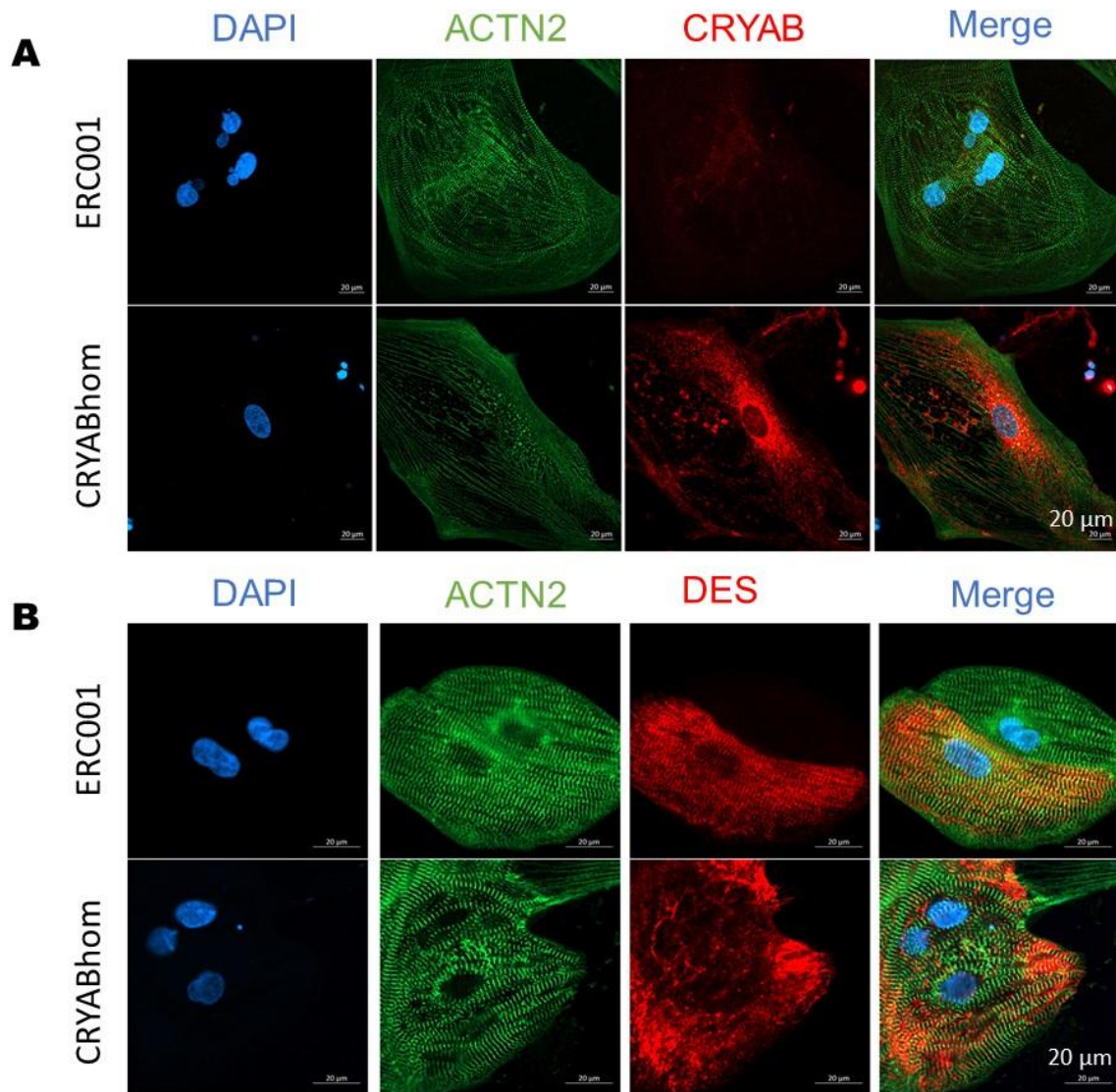


Figure 10. Representative images of CRYAB and DES in CRYABhom and ERC001 hiPSC-CMs by immunofluorescence analysis. (A) The distribution of CRYAB. The cells were fixed in 4% PFA and nuclei are depicted in blue (DAPI), ACTN2 in green and CRYAB in red. **(B)** The distribution of DES. The cells were fixed in 4% PFA and nuclei were stained with DAPI (blue), ACTN2 (green) and DES (red). Scale bar=20 μm (40x-objective). (This image was provided by Antonietta Fazio). Abbreviations: ACTN2, α -actinin 2; CMs, human induced pluripotent stem cell-derived cardiomyocytes; hiPSC, human induced pluripotent stem cell.

3.7 The autophagic flux was higher in 30-day-old CRYABhom than ERC001 hiPSC-CMs

Various studies found that the major markers of autophagy (LC3-II, p62) were quantified in protein of heart or cardiomyocyte by Western blot assay (Bhuiyan et al. 2013, Song et al. 2014,

Singh et al. 2017). We then evaluated whether the autophagic flux is altered in CRYAB^{hom} hiPSC-CMs. Thirty-day-old ERC001 and CRYAB^{hom} hiPSC-CMs were treated with bafilomycin A₁ (BAF; 50 nM in DMSO), which inhibits the fusion between the autophagosome and lysosome or DMSO, as baseline condition for 3 h or 24 h. Treatments were performed by Antonietta Fazio. Then, protein levels of the autophagic markers LC3-II and p62 were assessed by Western blot on the SDS protein fraction. The difference in the LC3-II protein levels between BAF-treated and DMSO-treated hiPSC-CMs represents the autophagic flux. **Figure 11A** shows the representative Western blots (LC3-II, p62; 12% SDS gel) performed on SDS fraction of CRYAB^{hom} and ERC001 hiPSC-CMs cultivated for 30 days. **Figure 11B** shows the quantification of LC3-II levels normalized to GAPDH or Ponceau after DMSO and BAF treatments. LC3-II level was lower in CRYAB^{hom} than in ERC001 hiPSC-CMs in DMSO conditions. LC3-II level was slightly higher in ERC001 than in CRYAB^{hom} hiPSC-CMs in BAF-treated conditions when normalized to GAPDH. No major difference was detected when normalized to Ponceau. However, LC3-II protein levels normalized to Ponceau were significantly higher in BAF-treated than in DMSO-treated in CRYAB^{hom} hiPSC-CMs. The difference in LC3-II levels between BAF-treated and DMSO-treated seems to be higher in CRYAB^{hom}, suggesting higher autophagic flux than in ERC001 hiPSC-CMs. **Figure 11C** shows the quantification of p62 protein levels normalized to GAPDH or Ponceau. Similar to LC3-II, p62 level were higher in BAF-treated than in DMSO-treated samples, without significant difference among the groups.

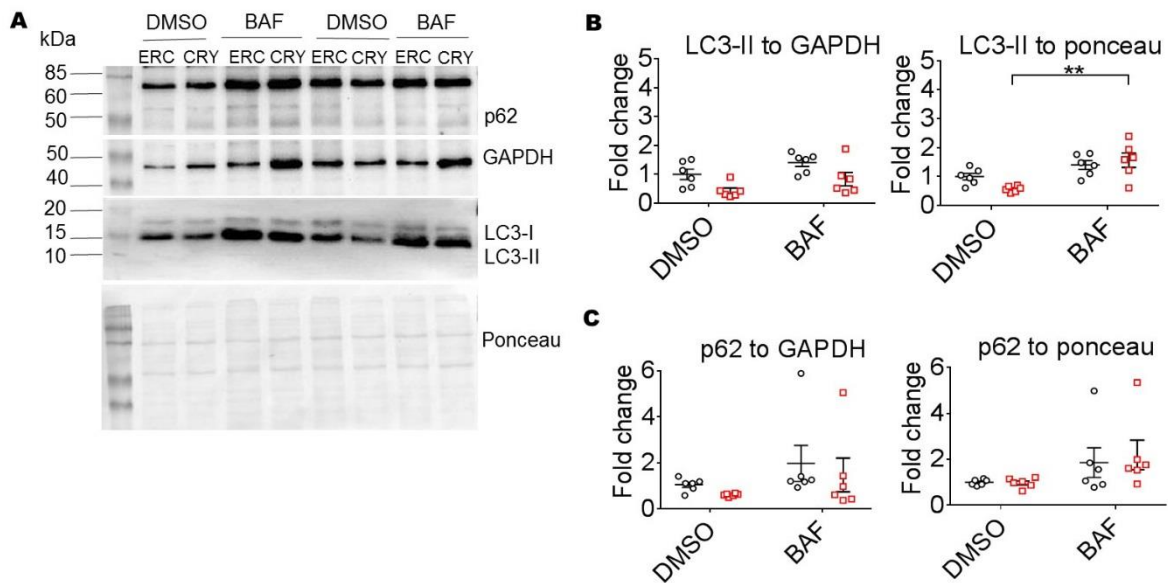


Figure 11. Evaluation of LC3-II and p62 protein levels in the CRYABhom and ERC001 hiPSC-CMs. **A)** Representative Western blot (LC3-II, p62; 12% SDS gel) of the SDS fraction of CRYABhom and ERC001 hiPSC-CMs with DMSO or BAF at 30 days. **(B & C)** Quantification of western blots. Black circles referred to ERC001 hiPSC-CMs and red square stood for CRYABhom hiPSC-CMs. Data are expressed as mean \pm SEM, with $^{***}P < 0.01$, two-way ANOVA with Tukey's multiple comparisons test. GAPDH and ponceau were applied as loading controls. Abbreviations: BAF, bafilomycin A₁; DMSO, dimethylsulfoxide; GAPDH, glyceraldehyde-3-phosphate dehydrogenase; hiPSC-CMs, human induced pluripotent stem cell-derived cardiomyocytes.

3.8 The autophagic flux did not differ between 60-day-old CRYABhom and ERC001 hiPSC-CMs

We then evaluated whether the autophagic flux differs in 60-day-old hiPSC-CMs. **Figure 12A** exhibits a representative Western blot for LC3-II and p62 performed on the SDS fraction of CRYABhom and ERC001 hiPSC-CMs with DMSO or BAF. There was a tendency for higher levels of both LC3-II and p62 after BAF, but no significant difference was observed between the groups (**Figure 12B, 12C**).

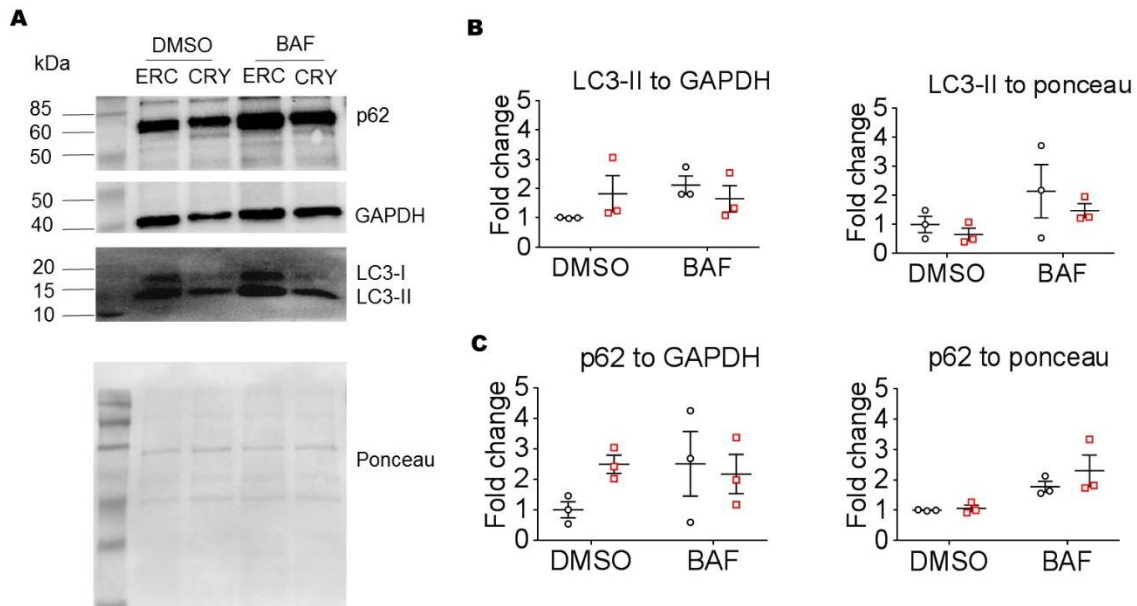


Figure 12. Evaluation of LC3-II and p62 protein levels in 60-day-old CRYABhom and ERC001 hiPSC-CMs. **A)** Representative western blot (LC3 II, p62; 12% SDS gel) of the SDS fraction of CRYABhom and ERC001 hiPSC-CMs with DMSO or BAF at 60 days. **B & C)** Quantification of Western blots. Black circles stood for ERC001 hiPSC-CMs and red square represented CRYABhom hiPSC-CMs. Data are expressed as mean \pm SEM and compared with the two-way ANOVA followed by Sidak's multiple comparisons test. GAPDH and ponceau were employed as loading controls. Abbreviations: BAF, bafilomycin A₁; DMSO, dimethylsulfoxide; hiPSC-CMs: human induced pluripotent stem cell-derived cardiomyocytes.

3.9 The UPS was impaired in 60-day-old CRYABhom hiPSC-CMs

To evaluate the activity of the UPS, both hiPSC-CM lines were transduced with GFPu. GFPu serves as a UPS reporter comprising of a short degron (CL1) fused to the green fluorescent protein (GFP) (Bence et al. 2005, McLendon et al. 2017)(Singh et al. 2021). When the UPS is inhibited or impaired, GFPu is not degraded and thus accumulates in cells. Both ERC001 and CRYABhom hiPSC-CMs were transduced with an adenovirus encoding GFPu at a multiplicity of infection (MOI) of 5 for 4 days, and then treated with DMSO or epoxomicin (EPO; 250 nM, for 15 h). Protein levels of GFPu and polyubiquitin were assessed by Western blot analysis.

Figure 13A shows a representative Western blot stained for GFP and ACTN2 performed on SDS protein fraction isolated from CRYABhom and ERC001 hiPSC-CMs treated with DMSO or EPO at 60 days. Protein level of GFPu (stained by the GFP antibody) was higher in CRYABhom than in ERC001 hiPSC-CMs in basal conditions, suggesting less UPS-mediated degradation. Inhibition of the proteasome with EPO increased the GFPu level in both cell lines and to a greater extent in CRYABhom.

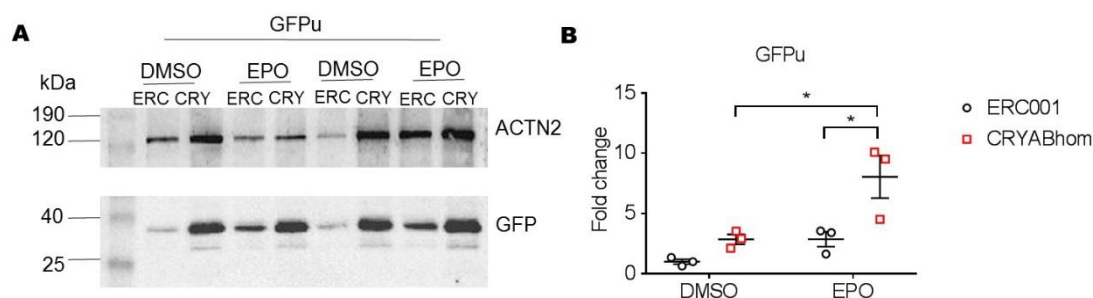


Figure 13. Western blot assay for GFPu in CRYABhom and ERC001 hiPSC-CMs. Sixty-day-old hiPSC-CMs were transduced with an adenovirus encoding the fluorescent UPS reporter GFPu at a MOI of 5 for 4 days. **A**) Representative Western blot stained with ACTN2 and GFP antibodies (10% SDS gel) of the SDS fraction isolated from CRYABhom and ERC001 hiPSC-CMs with DMSO or EPO (250 nM; 15 h) at 60 days. **B**) Quantification of GFPu protein levels normalized to ACTN2. Data are expressed as mean \pm SEM, with * $P < 0.05$, two-way ANOVA followed by Sidak's multiple comparisons test. ACTN2 was utilized as a loading control. Abbreviations: ACTN2, α -actinin 2; DMSO, dimethylsulfoxide; EPO, epoxomicin; MOI, Multiplicity of infection, hiPSC-CMs, human induced pluripotent stem cell-derived cardiomyocytes.

We then evaluated the polyubiquitinated protein level in the different samples and conditions. In basal conditions (DMSO), there was a tendency to higher level of polyubiquitinated proteins when normalized to Ponceau but not to GAPDH (**Figure 14**). Proteasome inhibition with EPO increased to a similar extent in both groups.

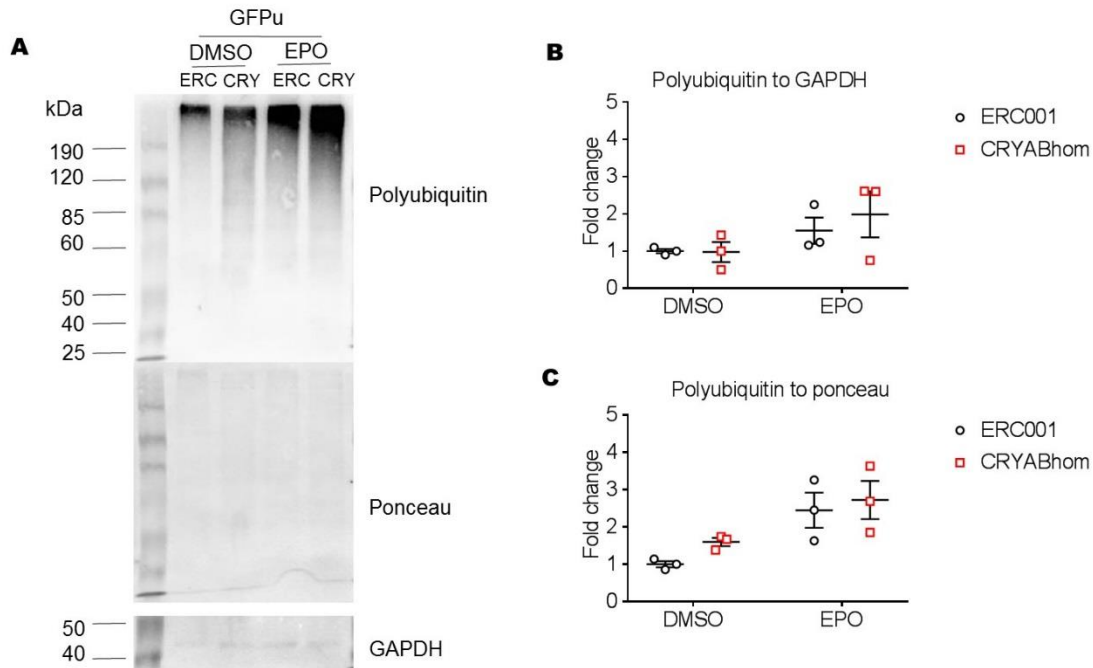


Figure 14. Western blot assay for polyubiquitinated proteins in CRYABhom and ERC001 hiPSC-CMs. **A)** Representative Western blot stained with anti-ubiquitin and anti-GAPDH antibodies (8% SDS gel) performed on the SDS fraction which was harvested from CRYABhom and ERC001 hiPSC-CMs treated with DMSO or EPO (250 nM; 15 h) at 60 days. **B & C)** Quantification of polyubiquitinated protein level. Data are expressed as mean \pm SEM and comparison between groups was performed with the two-way ANOVA followed by the Sidak's multiple comparisons test. GAPDH and Ponceau served as loading controls. Abbreviations: DMSO, Dimethylsulfoxide; EPO, epoxomicin; GAPDH, glyceraldehyde-3-phosphate dehydrogenase; hiPSC-CMs: human induced pluripotent stem cell-derived cardiomyocytes.

Collectively, the evaluation of both GFPu and polyubiquitinated proteins suggests that the UPS is impaired in the CRYABhom hiPSC-CMs, although more samples are required to validate these data.

4 Discussion

4.1 The main aim and result of this project

The major aim of this project was to characterize a novel human induced hiPSC-derived DRM model with the *CRYAB* R120G mutation, which was produced in the institute by using the CRISPR/Cas9 technique. As a result, a homozygous clone with *CRYAB* knock-in was found, in which two alleles in the CRYABhom cell line were determined. In addition, the protein levels of CRYAB and DES were lower in 30-day-old CRYABhom than in ERC001 hiPSC-CMs, however, the mRNA levels of *CRYAB* and *DES* did not differ significantly between the two cell lines. Additionally, intracellular protein aggregates of CRYAB and DES were observed in CRYABhom hiPSC-CMs but not in ERC001 hiPSC-CMs. Furthermore, the level of GFPu protein was much higher in CRYABhom hiPSC-CMs than that in the control group with and without UPS inhibitor, suggesting that the UPS is impaired in CRYABhom hiPSC-CMs. On the other hand, the level of LC3-II protein was significantly lower in CRYABhom hiPSC-CMs than in ERC001 hiPSC-CMs at 30 days with DMSO, but not with ALP inhibitor, which suggested that ALP was activated in CRYABhom hiPSC-CMs.

4.2 Advantages of the CRISPR/Cas9 gene editing tools

The CRISPR/Cas9 system as a versatile gene editing tool plays a critical role in research and also has huge potential for therapy of inherited diseases (Doudna and Charpentier 2014, Wilson and Gilbert 2018). The CRISPR/Cas9 system applies sgRNA to target DNA endonuclease Cas9 to specific DNA sequences, which can facilitate its specific cleavage (Jiang and Doudna 2017). Cas9-induced double-strand break can be repaired through two different mechanisms, non-homologous end joining (NHEJ) mechanisms, which can result in all sorts of mutations in the targeted DNA, or via homology directed repair (HDR), which used a donor DNA as template for homologous recombination (Gasiunas et al. 2012, Guernet and Grumolato 2017, Zhan et al. 2019). Cas9 offers a few advantages to conventional protein-guided genome editing tools including zinc finger nucleases (ZFNs) and transcription activator-like effector nucleases

(TALENs). It is only needed to design a complementary sgRNA but without a change of the nuclease Cas9. This is simpler than the full synthesis of a huge guiding protein such as in TALEN- or ZFN-based tools. In addition, with numerous sgRNAs targeting different genomic loci, these genomic loci can be edited in parallel by Cas9, which shows multiplexing of Cas9 system (Cong et al. 2013, Doudna and Charpentier 2014). The Cas9 tool also has the merit over RNA interference technology because the influences of RNA interference are non-specific, temporary and limited to reduce gene expression.

4.3 Advantages of hiPSC-CMs to study heart diseases

Shi et al. reviewed recent progress and applications of hiPSC technology for cardiac diseases (Shi et al. 2017). HiPSCs have been widely applied to construct disease model, to find new drug and to develop cell therapy. Furthermore, the application of Cas9 tool enabled rapid generation of genetically defined disease models by using hiPSCs. Therefore, it is promising to construct a hiPSC-derived DRM model with Cas9 technology. Some of the advantages of hiPSCs in the study of heart disease are described in the following. First, the utilization of hiPSC-CMs to study heart diseases has an advantage on rodent systems because of its human source (Lee et al. 2012). Additionally, hiPSC-CMs may have an advantage compared with immortalized cell lines due to their similar functional features to primary human cardiomyocytes, and can be produced unlimitedly in quantities (Navarrete et al. 2013). In addition, the application of hiPSC-CMs in the study of heart diseases does not have ethical constraints in establishment of cell lines in comparison to human embryonic stem cells-CMs (Khan et al. 2013).

In our study, a control hiPSC line (ERC001) was used to introduce the R120G (c.358A>G) mutation in *CRYAB* gene by CRISPR/Cas9 gene editing tool with the goal to define an in vitro phenotype of DRM and then to test therapeutics. The above advantages of hiPSC-CMs showed a high value of our hiPSC-derived DRM model. Heterozygous mutation was expected for our DRM model, however, only a homozygous clone was obtained by sequencing of the recombinant *CRYAB*-targeted hiPSC clone. To assess whether the introduced *CRYAB* mutation was homozygous and not correlated with a deletion of the other allele, qPCR assay was

conducted to detect the number of alleles in the CRYAB^{hom} hiPSC line and two alleles in the CRYAB^{hom} cell line were determined.

4.4 Protein levels and aggregation of CRYAB and DES in DRM models

Western blot assay was performed to determine the levels of CRYAB and DES in CRYAB^{hom} hiPSC-CMs and ERC001 hiPSC-CMs at 30 days. As indicated in **Figure 8 & Figure 10**, despite the lower protein levels of *CRYAB* and *DES* were observed by Western blot, we found both accumulation of CRYAB and DES aggregates by immunofluorescence in CRYAB^{hom} hiPSC-CMs. The possible causes are the following. Firstly, in spite of the aggregate formation of CRYAB and DES, the overall distributions of CRYAB and DES were reduced within CRYAB^{hom} hiPSC-CMs. On the other hand, the aggregation of CRYAB and DES may be impaired in the protein extraction, leading to the decline of CRYAB and DES based on Western blot assay. Other methods that may effectively extract protein of CRYAB and DES should be used to validate the protein levels of CRYAB and DES.

Limphong et al. established a DRM model using mouse iPSCs (miPSCs) (Limphong et al. 2013). The existing transgenic mice model was used to derive miPSCs by using tail tip fibroblasts and a few miPSC lines were produced from transgenic and non-transgenic mice. The result of the immunofluorescence analysis showed perinuclear aggregates of CRYAB in transgenic miPSC-CMs. On the other hand, the protein and mRNA levels of *CRYAB* were much higher in transgenic miPSC-CMs than in non-transgenic miPSC-CMs. Obviously, the result for the protein and mRNA levels of *CRYAB* in their model was different to our DRM model. It is promising that both above models may pave the way for further experiments to decipher the mechanisms and to test therapy for DRM. On the other hand, Ito et al. characterized the essence of transiently expressed R120G *CRYAB* with mammalian cell lines (Ito et al. 2003). The result of Western blot showed that mutation *CRYAB* was predominantly discovered in the insoluble fraction and wild-type *CRYAB* was mainly found in the soluble fraction in HeLa cells. In addition, the immunofluorescence analysis showed perinuclear aggregates of CRYAB in the HeLa cells with transiently expressed R120G *CRYAB* (Ito et al. 2003). The above study

suggested that an effective method should be used to isolate the proteins of the insoluble fraction in CRYAB^{hom} hiPSC-CMs in our study.

4.5 The UPS and ALP in DRM models

The PQC systems plays a key role in promoting protein folding as well as eliminating terminally misfolded proteins (Wang and Robbins 2006). The elimination of abnormal proteins is mainly mediated by the UPS (Wang and Robbins 2006) and ALP (Levine and Kroemer 2008). We used a fluorescent UPS reporter substrate GFPu, which is normally degraded by the UPS. Our data showed that the protein level of GFPu were higher in CRYAB^{hom} than in ERC001 hiPSC-derived cardiomyocyte with EPO, but not with DMSO, likely due to the low number of replicates. The result suggests that the UPS is impaired in CRYAB^{hom} hiPSC-CMs.

Evaluation of the ALP with a specific inhibitor of the fusion between autophagosome and lysosome, BAF, showed that the protein level of LC3-II was lower in CRYAB^{hom} than in ERC001 hiPSC-CMs, mainly with DMSO. Additionally, significant difference was discovered between CRYAB^{hom} hiPSC-CMs with DMSO and CRYAB^{hom} hiPSC-CMs with BAF when ponceau was used as loading control. The data suggested that high level of autophagic flux was found in the CRYAB^{hom} hiPSC-CMs at 30 days and autophagic flux can be inhibited by BAF, suggesting that *CRYAB* mutation generated a key effect on ALP in hiPSC-CMs. Liu et al. assessed the effect of mutant *DES* on the UPS in human embryonic kidney (HEK) cells that did not express desmin normally. The result showed that transient transfection of mutant *DES* but not wild type *DES* significantly increased GFPu protein levels in the GFPu stably transfected human embryonic kidney 293 (HEK293) cells based on Western blot assay, indicating that UPS impairment due to mutant *DES* can occur in a cell line, which did not express desmin normally, in addition they also found that the UPS was impaired in DRM mouse hearts (Liu et al. 2006). Tannous et al. showed that mutant CRYABR120G increased the abundance of autophagosomes in neonatal rat ventricular myocytes (Tannous et al. 2008). However, they did not measure the autophagic flux, so this study cannot conclude whether ALP was activated or inhibited. However, this study showed similar result to our study, so we believe that the ALP was also

activated. Collectively, the implication of UPS and ALP in CRYAB^{hom} hiPSC-CMs suggested a high value of our DRM model to further study the pathogenesis of DRM.

4.6 Limitations of our study

Some limitations of this experiment need to be further elaborated. Western blotting for CRYAB and DES was performed with ACTN2 as loading control, but the other two replicates did not perform well with ACTN2 as loading control maybe due to low loading protein, which were conducted using GAPDH as loading control. Therefore, quantification of the protein levels of CRYAB and DES in CRYAB^{hom} and ERC001 hiPSC-CMs should be performed with only GAPDH or only ACTN2 as loading controls for the 3 Western blots. In addition, the proteins were enough for only two replicates of the Western blotting for CRYAB and DES levels in ERC001 hiPSC-CMs with DMSO at 30 days, then ERC001 hiPSC-CMs without DMSO at 30 days were used for the replication of the Western blotting. Thus, quantification of the protein levels of CRYAB and DES should be assessed using ERC001 hiPSC-CMs with DMSO at 30 days for the 3 western blots. Importantly, we were not able to detect accumulated CRYAB and DES by Western blot assay and therefore, we may use another protocol for insoluble protein extraction or try a filter trap assay. Finally, another limitation of this study was the number of replicates used for the GFPu and ALP experiments.

5 Summary

Desmin-related (cardio-)myopathy (DRM) serves as a class of protein-misfolding diseases, characterized by conduction defects, skeletal muscle weakness and cardiomyopathy, which is caused by variants in desmin (*DES*) or α B-crystallin (*CRYAB*) and there is no specific therapy available. Typical biomarkers of DRM are irregular cell structure, the formation of protein aggregates and impairment of ubiquitin-proteasome system (UPS) and autophagy-lysosomal pathway (ALP). The aim of this study was to characterize a novel human induced pluripotent stem cell (hiPSC)-derived DRM model with the *CRYAB* c.358A>G (p.R120G) variant, which was created in the institute with the CRISPR/Cas9 gene editing tools.

The c.358A>G variant was produced in the *CRYAB* gene of a hiPSC control line (ERC001) by using the CRISPR/Cas9 technique (*CRYAB*hom). And then both hiPSC lines were differentiated into cardiomyocytes (CMs). A qPCR assay was performed to determine the number of alleles in the *CRYAB*hom cell line using genomic DNA (gDNA). The alterations of *CRYAB* and *DES* in *CRYAB*hom and ERC001 hiPSC-CMs (at 30 days) were assessed through immunofluorescence analysis. The RT-qPCR assay was performed to evaluate the mRNA levels of *CRYAB* and *DES* in *CRYAB*hom and ERC001 hiPSC-CMs at different time points. Western blot assay was conducted to assess the UPS function in *CRYAB*hom and ERC001 hiPSC-CMs (60 days old) which were transduced using a GFPu adenovirus as well as treated by using the inhibitor of UPS epoxomicin (EPO) or dimethylsulfoxide (DMSO). Western blot assays were performed to evaluate the function of ALP by autophagy hallmark LC3-II in *CRYAB*hom and ERC001 hiPSC-CMs (30 and 60 days old) with the treatment of the ALP inhibitor bafilomycin (BAF) A1 or DMSO.

A homozygous clone with *CRYAB* knock-in was identified in which two alleles in the *CRYAB*hom hiPSC line was determined. The protein levels of *CRYAB* and *DES* were markedly lower in *CRYAB*hom than in ERC001 hiPSC-CMs at 30 days, whereas the mRNA levels of

CRYAB and *DES* did not differ between the two cell lines. In addition, intracellular protein aggregates of *CRYAB* and *DES* were found in *CRYAB*hom hiPSC-CMs but not in ERC001 hiPSC-CMs. Additionally, the levels of GFPu protein were much higher in *CRYAB*hom hiPSC-CMs than in the control group with UPS inhibitor, suggesting that UPS in *CRYAB*hom hiPSC-CMs was impaired. Furthermore, the levels of LC3-II protein were significantly reduced in *CRYAB*hom hiPSC-CMs in comparison to ERC001 hiPSC-CMs at 30 days with DMSO, but not with ALP inhibitor, indicating that ALP was activated in *CRYAB*hom hiPSC-CMs.

We successfully established a novel hiPSC-derived DRM model, which may serve as a useful tool for future studies.

6 Zusammenfassung

Die Desmin-bedingte Myopathie gehört zu einer Klasse von Proteinfehlfaltungskrankheiten, und ist durch Erregungsleitungsstörungen, Skelettmuskelschwäche und Kardiomyopathie gekennzeichnet. Sie wird durch Varianten in Desmin (*DES*) oder α B-Crystallin (*CRYAB*) verursacht und es gibt keine spezifische Therapie. Typische Biomarker der Desmin-bedingten Myopathie sind eine veränderte Zellstruktur, die Bildung von Proteinaggregaten und eine Beeinträchtigung des Ubiquitin-Proteasom-Systems (UPS) und des Autophagie-lysosomalen Abbauweges (ALP). Ziel dieser Studie war es, ein neuartiges, aus menschlichen induzierten pluripotenten Stammzellen (hiPSC) abgeleitetes Modell der Desmin-bedingten Kardiomyopathie (DRM) mit der *CRYAB*-Variante c.358A>G (p.R120G) zu charakterisieren, das im Institut mit den CRISPR/Cas9-Gene Editing-Tools erzeugt wurde.

Die c.358A>G-Variante wurde im *CRYAB*-Gen einer hiPSC-Kontrolllinie (ERC001) mit Hilfe der CRISPR/Cas9-Technik (*CRYAB*_{hom}) erzeugt. Anschließend wurden beide hiPSC-Linien in Kardiomyozyten (CMs) differenziert. Ein qPCR-Test wurde durchgeführt, um die Anzahl der Allele in der *CRYAB*_{hom}-Zelllinie unter Verwendung genomischer DNA (gDNA) zu bestimmen. Die Veränderungen von *CRYAB* und *DES* in *CRYAB*_{hom} und ERC001 hiPSC-CMs (nach 30 Tagen) wurden mittels Immunfluoreszenzanalyse untersucht. RT-qPCR-Assays wurden durchgeführt, um die mRNA-Spiegel von *CRYAB* und *DES* in *CRYAB*_{hom} und ERC001 hiPSC-CMs zu verschiedenen Zeitpunkten zu bewerten. Western-Blot-Assays wurden durchgeführt, um die UPS-Funktion in *CRYAB*_{hom} und ERC001 hiPSC-CMs (60 Tage alt) zu bewerten, die mit einem GFPu-Adenovirus transduziert und mit dem UPS-Inhibitor Epoxomicin (EPO) oder DMSO behandelt worden waren. Western-Blot-Assays wurden durchgeführt, um die Funktion des ALPs über den Autophagie-Marker LC3-II in *CRYAB*_{hom} und ERC001 hiPSC-CMs (30 und 60 Tage alt) unter Behandlung mit dem ALP-Inhibitor Bafilomycin (BAF) A1 oder der Kontrolle DMSO zu bewerten.

Es wurde ein homozygoter Klon mit CRYAB-Knock-in identifiziert, bei dem zwei Allele in der hiPSC-Linie CRYABhom bestimmt wurden. Die Proteinkonzentrationen von CRYAB und DES waren nach 30 Tagen in CRYABhom deutlich niedriger als in ERC001 hiPSC-CMs, während sich die mRNA-Konzentrationen von *CRYAB* und *DES* zwischen den beiden Zelllinien nicht unterschieden. Darüber hinaus wurden intrazelluläre Proteinaggregate von CRYAB und DES in CRYABhom hiPSC-CMs gefunden, nicht aber in ERC001 hiPSC-CMs. Des Weiteren waren die Konzentrationen des GFPu-Proteins in CRYABhom hiPSC-CMs viel höher als in der Kontrollgruppe mit UPS-Inhibitor, was darauf hindeutet, dass die UPS in CRYABhom hiPSC-CMs beeinträchtigt war. Außerdem war der Gehalt an LC3-II-Protein in CRYABhom hiPSC-CMs im Vergleich zu ERC001 hiPSC-CMs nach 30 Tagen mit DMSO, aber nicht mit ALP-Inhibitor signifikant reduziert, was darauf hindeutet, dass ALP in CRYABhom hiPSC-CMs aktiviert wurde.

Wir haben erfolgreich ein neuartiges hiPSC-abgeleitetes DRM-Modell etabliert, das als nützliches Werkzeug für zukünftige Studien dienen kann.

7 References

- Bence, N. F., E. J. Bennett and R. R. Kopito (2005). "Application and analysis of the GFPu family of ubiquitin-proteasome system reporters." Methods Enzymol **399**: 481-490.
- Bhuiyan, M. S., J. S. Pattison, H. Osinska, J. James, J. Gulick, P. M. McLendon, J. A. Hill, J. Sadoshima and J. Robbins (2013). "Enhanced autophagy ameliorates cardiac proteinopathy." J Clin Invest **123**(12): 5284-5297.
- Breckwoldt, K., D. Letuffe-Brenière, I. Mannhardt, T. Schulze, B. Ulmer, T. Werner, A. Benzin, B. Klampe, M. C. Reinsch, S. Laufer, et al. (2017). "Differentiation of cardiomyocytes and generation of human engineered heart tissue." Nat Protoc **12**(6): 1177-1197.
- Clemen, C. S., F. Stöckigt, K. H. Strucksberg, F. Chevessier, L. Winter, J. Schütz, R. Bauer, J. M. Thorweihe, D. Wenzel, U. Schlötzer-Schrehardt, et al. (2015). "The toxic effect of R350P mutant desmin in striated muscle of man and mouse." Acta Neuropathol **129**(2): 297-315.
- Cong, L., F. A. Ran, D. Cox, S. Lin, R. Barretto, N. Habib, P. D. Hsu, X. Wu, W. Jiang, L. A. Marraffini, et al. (2013). "Multiplex genome engineering using CRISPR/Cas systems." Science **339**(6121): 819-823.
- Doudna, J. A. and E. Charpentier (2014). "Genome editing. The new frontier of genome engineering with CRISPR-Cas9." Science **346**(6213): 1258096.
- Gasiunas, G., R. Barrangou, P. Horvath and V. Siksnys (2012). "Cas9-crRNA ribonucleoprotein complex mediates specific DNA cleavage for adaptive immunity in bacteria." Proc Natl Acad Sci U S A **109**(39): E2579-2586.
- Goldfarb, L. G. and M. C. Dalakas (2009). "Tragedy in a heartbeat: malfunctioning desmin causes skeletal and cardiac muscle disease." J Clin Invest **119**(7): 1806-1813.
- Goldfarb, L. G., P. Vicart, H. H. Goebel and M. C. Dalakas (2004). "Desmin myopathy." Brain **127**(Pt 4): 723-734.
- Goudeau, B., A. Dagvadorj, F. Rodrigues-Lima, P. Nédellec, M. Casteras-Simon, E. Perret, S. Langlois, L. Goldfarb and P. Vicart (2001). "Structural and functional analysis of a new desmin variant causing desmin-related myopathy." Hum Mutat **18**(5): 388-396.
- Guernet, A. and L. Grumolato (2017). "CRISPR/Cas9 editing of the genome for cancer modeling." Methods **121-122**: 130-137.

Hershko, A. and A. Ciechanover (1998). "The ubiquitin system." Annu Rev Biochem **67**: 425-479.

Hnia, K., C. Ramspacher, J. Vermot and J. Laporte (2015). "Desmin in muscle and associated diseases: beyond the structural function." Cell Tissue Res **360**(3): 591-608.

Ito, H., K. Kamei, I. Iwamoto, Y. Inaguma, M. Tsuzuki, M. Kishikawa, A. Shimada, M. Hosokawa and K. Kato (2003). "Hsp27 suppresses the formation of inclusion bodies induced by expression of R120G alpha B-crystallin, a cause of desmin-related myopathy." Cell Mol Life Sci **60**(6): 1217-1223.

Jiang, F. and J. A. Doudna (2017). "CRISPR-Cas9 Structures and Mechanisms." Annu Rev Biophys **46**: 505-529.

Kabeya, Y., N. Mizushima, T. Ueno, A. Yamamoto, T. Kirisako, T. Noda, E. Kominami, Y. Ohsumi and T. Yoshimori (2000). "LC3, a mammalian homologue of yeast Apg8p, is localized in autophagosome membranes after processing." Embo j **19**(21): 5720-5728.

Kedia, N., K. Arhzaouy, S. K. Pittman, Y. Sun, M. Batchelor, C. C. Weihl and J. Bieschke (2019). "Desmin forms toxic, seeding-competent amyloid aggregates that persist in muscle fibers." Proc Natl Acad Sci U S A **116**(34): 16835-16840.

Khan, J. M., A. R. Lyon and S. E. Harding (2013). "The case for induced pluripotent stem cell-derived cardiomyocytes in pharmacological screening." Br J Pharmacol **169**(2): 304-317.

Klionsky, D. J., A. K. Abdel-Aziz, S. Abdelfatah, M. Abdellatif, A. Abdoli, S. Abel, H. Abeliovich, M. H. Abildgaard, Y. P. Abudu, A. Acevedo-Arozena, et al. (2021). "Guidelines for the use and interpretation of assays for monitoring autophagy (4th edition)(1)." Autophagy **17**(1): 1-382.

Lee, P., M. Klos, C. Bollensdorff, L. Hou, P. Ewart, T. J. Kamp, J. Zhang, A. Bizy, G. Guerrero-Serna, P. Kohl, et al. (2012). "Simultaneous voltage and calcium mapping of genetically purified human induced pluripotent stem cell-derived cardiac myocyte monolayers." Circ Res **110**(12): 1556-1563.

Levine, B. and G. Kroemer (2008). "Autophagy in the pathogenesis of disease." Cell **132**(1): 27-42.

Limphong, P., H. Zhang, E. Christians, Q. Liu, M. Riedel, K. Ivey, P. Cheng, K. Mitzelfelt, G. Taylor, D. Winge, et al. (2013). "Modeling human protein aggregation cardiomyopathy using murine induced pluripotent stem cells." Stem Cells Transl Med **2**(3): 161-166.

Liu, J., Q. Chen, W. Huang, K. M. Horak, H. Zheng, R. Mestril and X. Wang (2006). "Impairment of the ubiquitin-proteasome system in desminopathy mouse hearts." Faseb j **20**(2): 362-364.

McLendon, P. M., G. Davis, J. Gulick, S. R. Singh, N. Xu, N. Salomonis, J. D. Molkenin and J. Robbins (2017). "An Unbiased High-Throughput Screen to Identify Novel Effectors That Impact on Cardiomyocyte Aggregate Levels." Circ Res **121**(6): 604-616.

Mizushima, N. and D. J. Klionsky (2007). "Protein turnover via autophagy: implications for metabolism." Annu Rev Nutr **27**: 19-40.

Mizushima, N., B. Levine, A. M. Cuervo and D. J. Klionsky (2008). "Autophagy fights disease through cellular self-digestion." Nature **451**(7182): 1069-1075.

Mosqueira, D., I. Mannhardt, J. R. Bhagwan, K. Lis-Slimak, P. Katili, E. Scott, M. Hassan, M. Prondzynski, S. C. Harmer, A. Tinker, et al. (2018). "CRISPR/Cas9 editing in human pluripotent stem cell-cardiomyocytes highlights arrhythmias, hypocontractility, and energy depletion as potential therapeutic targets for hypertrophic cardiomyopathy." Eur Heart J **39**(43): 3879-3892.

Navarrete, E. G., P. Liang, F. Lan, V. Sanchez-Freire, C. Simmons, T. Gong, A. Sharma, P. W. Burrige, B. Patlolla, A. S. Lee, et al. (2013). "Screening drug-induced arrhythmia [corrected] using human induced pluripotent stem cell-derived cardiomyocytes and low-impedance microelectrode arrays." Circulation **128**(11 Suppl 1): S3-13.

Paquet, D., D. Kwart, A. Chen, A. Sproul, S. Jacob, S. Teo, K. M. Olsen, A. Gregg, S. Noggle and M. Tessier-Lavigne (2016). "Efficient introduction of specific homozygous and heterozygous mutations using CRISPR/Cas9." Nature **533**(7601): 125-129.

Ravid, T. and M. Hochstrasser (2008). "Diversity of degradation signals in the ubiquitin-proteasome system." Nat Rev Mol Cell Biol **9**(9): 679-690.

Roberts, B., A. Haupt, A. Tucker, T. Grancharova, J. Arakaki, M. A. Fuqua, A. Nelson, C. Hookway, S. A. Ludmann, I. A. Mueller, et al. (2017). "Systematic gene tagging using CRISPR/Cas9 in human stem cells to illuminate cell organization." Mol Biol Cell **28**(21): 2854-2874.

Roberts, E. A. and V. Deretic (2008). "Autophagic proteolysis of long-lived proteins in nonliver cells." Methods Mol Biol **445**: 111-117.

Schlossarek, S., N. Frey and L. Carrier (2014). "Ubiquitin-proteasome system and hereditary cardiomyopathies." J Mol Cell Cardiol **71**: 25-31.

Selcen, D. and A. G. Engel (2004). "Mutations in myotilin cause myofibrillar myopathy." Neurology **62**(8): 1363-1371.

Shi, Y., H. Inoue, J. C. Wu and S. Yamanaka (2017). "Induced pluripotent stem cell technology: a decade of progress." Nat Rev Drug Discov **16**(2): 115-130.

Singh, S. R., M. Meyer-Jens, E. Alizoti, W. C. Bacon, G. Davis, H. Osinska, J. Gulick, S. Reischmann-Düsener, E. Orthey, P. M. McLendon, et al. (2021). "A high-throughput screening identifies ZNF418 as a novel regulator of the ubiquitin-proteasome system and autophagy-lysosomal pathway." Autophagy **17**(10): 3124-3139.

Singh, S. R., A. T. L. Zech, B. Geertz, S. Reischmann-Düsener, H. Osinska, M. Prondzynski, E. Krämer, Q. Meng, C. Redwood, J. van der Velden, et al. (2017). "Activation of Autophagy Ameliorates Cardiomyopathy in Mybpc3-Targeted Knockin Mice." Circ Heart Fail **10**(10).

Smalle, J. and R. D. Vierstra (2004). "The ubiquitin 26S proteasome proteolytic pathway." Annu Rev Plant Biol **55**: 555-590.

Song, L., M. Su, S. Wang, Y. Zou, X. Wang, Y. Wang, H. Cui, P. Zhao, R. Hui and J. Wang (2014). "MiR-451 is decreased in hypertrophic cardiomyopathy and regulates autophagy by targeting TSC1." J Cell Mol Med **18**(11): 2266-2274.

Tanaka, K. (2009). "The proteasome: overview of structure and functions." Proc Jpn Acad Ser B Phys Biol Sci **85**(1): 12-36.

Tannous, P., H. Zhu, J. L. Johnstone, J. M. Shelton, N. S. Rajasekaran, I. J. Benjamin, L. Nguyen, R. D. Gerard, B. Levine, B. A. Rothermel, et al. (2008). "Autophagy is an adaptive response in desmin-related cardiomyopathy." Proc Natl Acad Sci U S A **105**(28): 9745-9750.

van Spaendonck-Zwarts, K. Y., L. van Hessem, J. D. Jongbloed, H. E. de Walle, Y. Capetanaki, A. J. van der Kooi, I. M. van Langen, M. P. van den Berg and J. P. van Tintelen (2011). "Desmin-related myopathy." Clin Genet **80**(4): 354-366.

Vicart, P., A. Caron, P. Guicheney, Z. Li, M. C. Prevost, A. Faure, D. Chateau, F. Chapon, F. Tome, J. M. Dupret, et al. (1998). "A missense mutation in the alphaB-crystallin chaperone gene causes a desmin-related myopathy." Nat Genet **20**(1): 92-95.

Voges, D., P. Zwickl and W. Baumeister (1999). "The 26S proteasome: a molecular machine designed for controlled proteolysis." Annu Rev Biochem **68**: 1015-1068.

Vorgerd, M., P. F. van der Ven, V. Bruchertseifer, T. Löwe, R. A. Kley, R. Schröder, H.

- Lochmüller, M. Himmel, K. Koehler, D. O. Fürst, et al. (2005). "A mutation in the dimerization domain of filamin c causes a novel type of autosomal dominant myofibrillar myopathy." Am J Hum Genet **77**(2): 297-304.
- Wang, X., H. Osinska, R. Klevitsky, A. M. Gerdes, M. Nieman, J. Lorenz, T. Hewett and J. Robbins (2001). "Expression of R120G-alphaB-crystallin causes aberrant desmin and alphaB-crystallin aggregation and cardiomyopathy in mice." Circ Res **89**(1): 84-91.
- Wang, X. and J. Robbins (2006). "Heart failure and protein quality control." Circ Res **99**(12): 1315-1328.
- Wilson, R. C. and L. A. Gilbert (2018). "The Promise and Challenge of In Vivo Delivery for Genome Therapeutics." ACS Chem Biol **13**(2): 376-382.
- Yim, W. W. and N. Mizushima (2020). "Lysosome biology in autophagy." Cell Discov **6**: 6.
- Zech, A. T. L., S. R. Singh, S. Schlossarek and L. Carrier (2020). "Autophagy in cardiomyopathies." Biochim Biophys Acta Mol Cell Res **1867**(3): 118432.
- Zhan, T., N. Rindtorff, J. Betge, M. P. Ebert and M. Boutros (2019). "CRISPR/Cas9 for cancer research and therapy." Semin Cancer Biol **55**: 106-119.
- Zolk, O., C. Schenke and A. Sarikas (2006). "The ubiquitin-proteasome system: focus on the heart." Cardiovasc Res **70**(3): 410-421.

8 List of tables

Table 1: PCR mixture	12
Table 2: PCR program for genomic DNA amplification	12
Table 3: PCR primers	13
Table 4: Agarose gel mixture	13
Table 5: Program for cDNA synthesis	15
Table 6: Components for cDNA synthesis	15
Table 7: Program for qPCR	16
Table 8: Primers for qPCR	16
Table 9: Components of qPCR	16
Table 10: SDS buffer	18
Table 11: Primary and secondary antibodies for Western blot	20

9 List of figures

Figure 1: Molecular cytoarchitecture of myocyte, key proteins associated with cardiac and skeletal myopathies	7
Figure 2. A scheme for protein quality control.	8
Figure 3. A flow diagram for Western blot of the cells	18
Figure 4. Agarose gel electrophoresis of genomic PCR products of the selected hiPSC clones.	22
Figure 5. Sequencing of the recombinant <i>CRYAB</i> -targeted hiPSC clone.	23
Figure 6. qPCR assay for determination of the allele number in the <i>CRYAB</i> ^{hom} hiPSC line.	25
Figure 7. Western blot assay for <i>CRYAB</i> and <i>DES</i> protein levels of ERC001 hiPSCs and hiPSC-CMs.	26
Figure 8. Quantification of the protein levels of <i>CRYAB</i> and <i>DES</i> in <i>CRYAB</i> ^{hom} and ERC001 hiPSC-CMs at 30 days.	27
Figure 9. Determination of mRNA levels of <i>CRYAB</i> and <i>DES</i> in <i>CRYAB</i> ^{hom} and ERC001 hiPSC-CMs at different time points.	28
Figure 10. Representative images of <i>CRYAB</i> and <i>DES</i> in <i>CRYAB</i> ^{hom} and ERC001 hiPSC-CMs by immunofluorescence analysis.	30
Figure 11. Evaluation of LC3-II and p62 protein levels in the <i>CRYAB</i> ^{hom} and ERC001 hiPSC-CMs.	32
Figure 12. Evaluation of LC3-II and p62 protein levels in 60-day-old <i>CRYAB</i> ^{hom} and ERC001 hiPSC-CMs	33
Figure 13. Western blot assay for GFPu in <i>CRYAB</i> ^{hom} and ERC001 hiPSC-CMs.	34
Figure 14. Western blot assay for polyubiquitinated proteins in <i>CRYAB</i> ^{hom} and ERC001 hiPSC-CMs.....	35

10 Supplement

10.1 Abbreviations

C°: Degree celsius

µg: Micrograms

µL: Microliter

ACTN2: α -actinin 2

ALP: Autophagy-lysosomal pathway

APS: Ammonium persulfate

BAF: Bafilomycin A₁

bp: Base pair

BSA: bovine serum albumin

Cas: CRISPR-associated

cDNA: Complementary deoxyribonucleic acid

CRISPR: Clustered regularly interspaced short palindromic repeat

CRYAB: α B-crystallin gene or mRNA

CRYAB^{R120G}: Mutated α B-crystallin

*CRYAB*_{hom}: *CRYAB* homozygous variant c.358A>G (p.R120G)

DES: DES gene or mRNA

DMSO: Dimethylsulfoxide

DNA: deoxyribonucleic acid

DRM: DES-related cardiomyopathy

DTT: dithiothreitol

ECL: electrochemiluminescence

EDTA: Ethylenediaminetetraacetic acid

EPO: Epoxomicin

et al.: Et alii (and others)

FLNC: filamin C

GAPDH: glyceraldehyde-3-phosphate dehydrogenase

gDNA: Genomic DNA

GFP: Green fluorescence protein

GFPu: Green fluorescence protein with a short degron, CL1, fused to the COOH-terminus.

h: Hour

HDR: homology directed repair

HEK: human embryonic kidney

hiPSC: human induced pluripotent stem cell

hiPSC-CMs: human induced pluripotent stem cell-derived cardiomyocytes

IgG: Immunoglobulin G

kb: Kilobase

KDa: Kilodalton

LC3: Microtubule-associated protein light chain 3

M: Molar

mA: Milliampere

MgCl₂: Magnesium chloride

Min: Minute

mm: Millimetre

mM: Millimolar

MOI: Multiplicity of infection

MYOT: myotilin

mRNA: Messenger RNA

NaF: sodium fluoride

NC: Nitrocellulose

NCBI: National Centre for Biotechnology Information

ng: Nanogram

NHEJL: non-homologous end joining

PCR: Polymerase chain reaction

PFA: paraformaldehyde

pH: -Log₁₀ hydrogen ion concentration

PQC: Protein quality control

PVDF: Polyvinyl-difluoride

qPCR: Quantitative PCR

RNA: Ribonucleic acid

RNP: Ribonucleic protein

rpm: Revolutions per minute

RT-qPCR: Reverse transcription- quantitative polymerase chain reaction

SDS: Sodium dodecyl sulfate

SDS-PAGE: Sodium dodecyl sulfate polyacrylamide gel electrophoresis

SEM: Standard error of the mean

sgRNA: single guide RNA

ssODN: single-stranded oligodeoxynucleotide

TAE: Tris-acetate EDTA

TALENs: transcription activator-like effector nucleases

TBS: Tris-buffered saline

TBS-T: Tris buffered saline with Tween 20

TEMED: Tetramethylethylenediamine;

Tris: Tris(hydroxymethyl)aminomethanen

UKE: Universitätsklinikum Hamburg-Eppendorf

UPS: ubiquitin-proteasome system

V: Volt

W: Watt

ZFNs: zinc finger nucleases

10.2 Materials

10.21 Chemicals, reagents, drugs etc

Chemicals, drugs, reagents etc.	Manufacturer
Acrylamide (40%)	BIORAD

Agarose	Invitrogen
APS (10%)	BIORAD
BAF	SIGMA
BenchMark Protein Ladder	Thermo Fisher Scientific
Chloroform	J.T.BAKER
DNA loading dye, 6x	ThermoScientific
DMSO	SIGMA
DTT	Sigma-Aldrich
ECL	ThermoScientific
EPO	CALBIOCHEM
Ethanol	ROTH
GeneRuler 1 kb DNA Ladder	Fermentas
Hoechst	Thermo Fisher Scientific
Isopropanol	EMSURE
Paraformaldehyde	Merck
Methanol	J.T.BAKER
Midori Green Advance DNA Stain	NIPPON Genetics EUROPE Gmhff
Milk powder	ROTH
Ponceau S	Sigma
Protease inhibitor tablet	Roche
RNAse-free water	Promega
SDS (10%)	ROTH
TBS	Sigma-Aldrich
Tris	MERCK
TRIzol Reagent	Ambin
Tween 20	Sigma-Aldrich
Urea	MERCK

10.22 Consumable materials

Product	Manufacturer
Blotting paper (Whatman TM 3mm)	GE Healthcare
Falcon tubes (15 and 50 mL)	Sarstedt AG & Co.
Latex gloves	Kimberly-Clark
Microtubes (1.5, 2.0 mL)	Sarstedt AG & Co.
Nitrile gloves	Ansell
Nitrocellulose membrane	Amersham TM
PCR tubes	Sarstedt AG & Co.
Pipette tips (for 10, 100 and 1000 uL pipettes)	Sarstedt AG & Co.
PVDF membrane	GE Healthcare

Serological pipettes (2, 5, 10 and 25 mL)	Sarstedt AG & Co.
---	-------------------

10.23 Laboratory equipment

Product	Manufacturer
Accu-jet pipetting aid	Brand GmbH
Benchtop centrifuge	Sarstedt AG & Co.
Blotting system (Mini Trans-Blot cell)	Bio-Rad
Centrifuge (5810 R)	Eppendorf AG
ChemiDoc	Bio-Rad
Electrophoresis system	Bio-Rad
Ice machine	Scotsman
Magnetic stirrer	Janke & Kunkel GmbH
PCR cycler (GeneAmpR PCR system 9700)	Eppendorf AG
Pipettes (10,100,1000 uL)	Eppendorf AG
Sonication device	Bandelin Sonopuls HD 2200
Spectrophotometer (NanoDrop™ ND-1000)	Thermo Fisher Scientific
TaqManABI Prism7900 HT sequence detection system with ABI 7900HT SDS Qiagen	Applied Biosystems
Thermomixer comfort	Eppendorf AG
Tube roller	Benchmark Scientific
Ultra-pure water system Milli-Q plus VI	Millipore
Vortex mixer	Janke & Kunkel GmbH

10.24 Kits

Product	Manufacturer
Dneasy Blood Tissue it (250)	QIAGEN
iScript™ cDNA Synthesis Kit #K1708841	Bio-Rad
PCR Kit	Thermo Fisher Scientific
QIAquick PCR Purification Kit (250)	QIAGEN
qPCR kit #K0223	ThermoScientific
Qubit™ Protein Assay Kit,500 assays	Invitrogen

10.25 Software

Software	Manufacturer
----------	--------------

EndNote	Thomson Corporation
GraphPad Prism software 8.0	GraphPad Software
Image J	National Institute of Health
Image Lab Version 5.2.1	Bio-Rad Laboratories

11 Acknowledgements

I would like to express my deepest gratitude to everyone for their guidance and support towards my thesis.

First and foremost, I would like to thank Prof. Dr. Lucie Carrier and Prof. Dr. Thomas Eschenhagen for providing me the opportunity to perform the experiments for my MD in the Institute of Experimental Pharmacology and Toxicology, and for the ceaseless supervision, guidance as well as support of Prof. Dr. Lucie Carrier.

Next, I would like to thank my second supervisor Singh Sonia for her detailed and key evaluation of my work and scientific constructive supervision for my project. In addition, she also taught me a lot of laboratory skills and writing skill which were very critical for my thesis. In addition, my special gratitude to Niels Pietsch for his profound scientific knowledge and scientific advice which were critical in my work.

Furthermore, my special gratitude to Niels and Antonietta: Niels performed the establishment of the CRYAB^{hom} hiPSC lines, including the design of the sgRNA and cardiac differentiation Antonietta performed the cardiomyocyte differentiation and all experiments required to evaluate the UPS and ALP in these cells with the different treatments, and finally also the preparation of the cell pellets for my analysis.

Next, I am thankful to Dr. Ellen Orthey. She supervised me and taught me a lot of laboratory skills and she was very patient and friendly with me. In every aspect, she was a helping hand, helping me to progress in my work.

Finally, I am thankful to my dear colleagues and friends for the friendly and family-like nice atmosphere: Elisabeth Kraemer, Erda Alizoti, Moritz Meyer-Jens, Saskia Schlossarek, Antonietta Fazio, Bangfen Pan, Ping Lai.

12 Curriculum Vitae



Jiancheng Cheng

Emil-Andresen-Straße 34c, 22529 Hamburg

Phone: +49 1625196879

Mail: jiancheng.cheng@outlook.com

Date of Birth: 5th April 1989, Kaifeng of China

Parents: Shuangdun Cheng, peasant
Wenzhi Gao, peasant

Siblings: Jianwei Cheng, peasant

Education and Work experience:

9/2010-6/2015: Jining Medical College in Jining city, Shandong province of China. I had a combined grasp of theoretical knowledge. During my internship, I paid attention to the combination of theory and practice. I developed a strong interest both theoretical knowledge and practice. I took part in some studies in school laboratories on mice, rabbits and toads.

9/2015-6/2018: Department of Cardiovascular Surgery, Union Hospital, Tongji Medical College, Huazhong University of Science and Technology, Wuhan 430022, China. During the master's degree, I read a lot of literature and had strong reading and writing skills. Proficient in Western blotting and PCR techniques, and had a deep understanding of EVG, Masson and HE staining techniques as well as cell apoptosis techniques. I independently completed the research on the role of ACTA2 in the pathogenesis of aneurysms, and jointly completed the research on the role of cab-1 in the pathogenesis of aortic dissection aneurysms.

Since 2018: Department of Cardiothoracic Surgery, Zhengzhou Central Hospital, Zhengzhou University, Zhengzhou, China. I am proficient in the treatment of inpatients with cardiac diseases and other diseases in other departments, as well as thoracentesis, tracheal intubation and other operational techniques. In addition, I have also participated in hundreds of major cardiovascular surgeries as an assistant.

Since 12/2020: Study in Universitätsklinikum Hamburg-Eppendorf, Martinistraße 52, 20246 Hamburg, Institut für Experimentelle Pharmakologie und Toxikologie, Germany.

Publications:

1 Jiancheng Cheng, Xianwu Zhou, Xionggang Jiang, Tucheng Sun. Deletion of ACTA2 in mice promotes angiotensin II induced pathogenesis of thoracic aortic aneurysms and dissections. *J Thorac Dis.* 2018; 10(8):4733-4740.

2 Xianwu Zhou¹, Jiancheng Cheng², Zerui Chen¹, Huadong Li³, Shu Chen³, Fei Xu⁴, Ruixin Fan¹, Jian Zhuang⁵, Tucheng Sun⁶ Role of c-Abl in Ang II-induced aortic dissection formation: potential regulatory efficacy on phenotypic transformation and apoptosis of VSMCs. *Life Sci.* 2020 Sep 1;256:117882.

13 Eidesstattliche Versicherung

Ich versichere ausdrücklich, dass ich die Arbeit selbständig und ohne fremde Hilfe verfasst, andere als die von mir angegebenen Quellen und Hilfsmittel nicht benutzt und die aus den benutzten Werken wörtlich oder inhaltlich entnommenen Stellen einzeln nach Ausgabe (Auflage und Jahr des Erscheinens), Band und Seite des benutzten Werkes kenntlich gemacht habe.

Ferner versichere ich, dass ich die Dissertation bisher nicht einem Fachvertreter an einer anderen Hochschule zur Überprüfung vorgelegt oder mich anderweitig um Zulassung zur Promotion beworben habe.

Ich erkläre mich einverstanden, dass meine Dissertation vom Dekanat der Medizinischen Fakultät mit einer gängigen Software zur Erkennung von Plagiaten überprüft werden kann.

Unterschrift: